Electron Paramagnetic Resonance of Fe^{3+} in Guanidinium Aluminum Sulfate Hexahydrate and Di-Ammonium Indium Pentachloride Monohydrate

George Russell Sharp

A Thesis
in
The Department
of
Physics

Presented in Partial Fulfillment of the Requirements
for the degree of Doctor of Philosophy
Concordia University
Montreal, Quebec, Canada

August, 1976

TABLE OF CONTENTS

ABSTRACT

George Russell Sharp

Electron Paramagnetic Resonance of Fe^{3+} in Guanidinium
Aluminum Sulfate Hexahydrate and Di-Ammonium
Indium Pentachloride Monohydrate

Electron paramagnetic resonance measurements on Fe^{3+} in guanidinium aluminum sulfate hexahydrate, $C(NH_2)_3Al(SO_4)_2 \cdot 6H_2O$ at 300 K, 79.0 K and 1.6 K, and in di-ammonium indium pentachloride monohydrate, $(NH_4)_2InCl_5 \cdot H_2O$ at 295 K, at X-band frequencies are presented. The values of all the spin Hamiltonian parameters are deduced from the data using a rigorous least-squares fitting procedure, in a simultaneous fitting of the data corresponding to ten orientations of the static magnetic field.

For Fe^{3+} in $C(NH_2)_3Al(SO_4)_2 \cdot 6H_2O$ the sign of the zero field splitting parameter b_2^0, as determined from liquid helium data, is found to be negative. In particular, the following values for the g-tensor and b_2^0 are found. At 295 K, for site I: $g_{zz} = 2.001 \pm .003$, $g_{xx} = 2.004 \pm .003$, $b_2^0 = -8.622 \pm .008$ gHz; for site II: $g_{zz} = 2.002 \pm .003$, $g_{xx} = 2.002 \pm .003$, $b_2^0 = -8.499 \pm .008$ gHz. At 1.6 K for site I: $g_{zz} = 1.994 \pm .003$, $g_{xx} = 1.992 \pm .003$, $b_2^0 = -8.931 \pm .008$ gHz; for site II: $g_{zz} = 1.996 \pm .003$, $g_{xx} = 1.997 \pm .003$, $b_2^0 = -8.808 \pm .008$ gHz.

For Fe^{3+} in $(NH_4)_2InCl_5 \cdot H_2O$ the following values for the

g-tensor, b_2^0 and b_2^2 are found. At 295 K, for site I: $g_{zz} = 2.014 \pm .003$, $g_{xx} = 2.016 \pm .003$, $g_{yy} = 2.014 \pm .003$, $b_2^0 = -4.570 \pm .008$ gHz, $b_2^2 = 2.545 \pm .008$ gHz; for site II: $g_{zz} = 2.015 \pm .003$, $g_{xx} = 2.015 \pm .003$, $g_{yy} = 2.008 \pm .003$, $b_2^0 = -4.563 \pm .008$ gHz, $b_2^2 = 2.547 \pm .008$ gHz. As well it is found that the Z and X-axes for the two inequivalent sites lie in the ac plane, with the Z-axes making angles of $\pm$ (40.00 $\pm$ 0.25°) with the a-axes.

ACKNOWLEDGEMENTS

The author wishes to express deep gratitude to Dr. S. K. Misra for proposing this study and for his continued interest, patience and invaluable assistance. He gratefully acknowledges the encouragement received from Dr. B. Frank and Dr. R. Verschingel, Dean of Science.

The author is thankful to the Department of Physics and the Faculty of Science for the facilities provided him for this research. He is also indebted to Mr. J. Blaison, Mr. A. Christodoulopoulos and Mr. J. Loustau for their very helpful technical assistance. The extensive use of the Concordia University CDC-6400 computer and the cooperation of the staff of the Computer Centre are gratefully acknowledged.

The author especially appreciates the encouragement received from his parents, his wife Berenice, and Mr. and Mrs. J. H. Morrison. As well he is thankful to his son, Anthony, for keeping him company on late evenings.

Grateful acknowledgement is also made of the remuneration received during the author's appointment as graduate research assistant for several years from Dr. S. K. Misra's N. R. C. grant (No. A4485).

CHAPTER I

INTRODUCTION

The purpose of this work was to obtain detailed information about the electron paramagnetic resonance (EPR) spectra of Fe^{3+} in guanidinium aluminum sulfate hexahydrate (GASH) and in di-ammonium indium pentachloride monohydrate, $(NH_4)_2InCl_5 \cdot H_2O$. An accurate knowledge of the spin Hamiltonian parameters, among other things, is required for the calculation of dynamic nuclear orientation and the analysis of Mossbauer data. The motivation for the present study was to find samples suitable for the study of the detection of dynamically oriented Fe nuclei by the Mossbauer effect.[1,2]

The electron paramagnetic resonance spectra of Fe^{3+} in GASH has been investigated by Brock et. al.[3] and Schwartz et. al.[4] Their parameters have been calculated using four lines at an X-band frequency along one axis of the g-tensor. The values of the spin Hamiltonian parameters quoted here are calculated using a procedure employing the least-squares fitting as developed for the analysis of EPR data by Misra,[5] which simultaneously considers magnetic resonance transitions obtained for any number of orientations of the static magnetic field. Approximately forty-five lines at ten different orientations are taken into account to calculate the parameters of the spin

Hamiltonian. The spectra were obtained at 295 K, 78.99 K and 1.61 K. The low temperature data being used to determine the absolute sign of the zero field splitting parameter B_2^0. This in-depth study has produced several important results:(i) the previous identifications of observed magnetic resonance transitions are found incorrect, and hence (ii) the parameters which characterize the EPR spectra quoted here are substantially different from those quoted in Refs. 3 and 4.

The Fe^{3+} ion in $(NH_4)_2InCl_5 \cdot H_2O$ has previously been studied by Wesemeyer[6] and by Amitay[7] but has not been published. The spectra was investigated at room temperature and analyzed in a similar fashion to Fe^{3+} in GASH. Previous studies calculated the parameters using the data obtained for the magnetic field orientation along one axis of the g-tensor whereas this study used ten orientations of the static magnetic field including the X, Y, and Z directions of the g-tensor. Therefore, these calculations provide a more accurate set of parameters. In addition, the EPR data is used to substantiate the microscopic crystalline structure of $(NH_4)_2InCl_5 \cdot H_2O$.

In chapter II the relevant theory and the spin Hamiltonian for each sample are presented. The details of the EPR spectrometer are given in chapter III. Chapter IV describes the procedure for the analysis of the data. Chapter V and VI contain the analysis of the data for Fe^{3+} in guanidinium aluminum sulfate hexahydrate. and di-ammonium indium pentachloride monohydrate respectively.

CHAPTER II

SPIN HAMILTONIAN FOR Fe^{3+} in GASH AND $(NH_4)_2InCl_5 \cdot H_2O$

Fe^{3+} has five electrons in the 3d shell (electronic spin $S = 5/2$) and the total orbital angular momentum of the ground state is $\bar{L} = 0$. If this was purely the case, in the absence of a magnetic field the sextet would have no splitting and the paramagnetic resonance spectrum would be remarkably simple. However in zero magnetic field the levels fall into three Kramers doublets indicating that the lattice ground state of these ions is not a pure S state but has small amounts of higher states admixed into it which leads to a more complex magnetic resonance spectrum.[8]

The spin Hamiltonian for Fe^{3+} contains terms representing the Zeeman interaction of the magnetic electrons with an external magnetic field and level splittings due to indirect effects of the crystal field. As well there may be terms representing the hyperfine structure due to the presence of a nuclear magnetic dipole moment which is non-zero for Fe^{57} for which $I = 1/2$, and the Zeeman interaction of the nuclear moment with the external field.

The electronic Zeeman interaction may be written as

$$H_{Zee} = \beta\,(\bar{H} \cdot \bar{\bar{g}} \cdot \bar{S}) \qquad (1)$$

where g is the g-tensor, H is the magnetic field, S is the electronic spin and β is the Bohr magneton.

The effects of the crystalline electric field arise from basically octahedral, tetrahedral or cubic array of surrounding negative charges or ligands. The nearest-neighbour ions dominate in determining the crystal potential. Ordinarily the surrounding charges are axially distorted with a tetragonal or trigonal axis of symmetry. The crystalline potential can be expressed as[9]

$$V(r\theta\phi) = \sum_{\ell=0}^{\infty} \sum_{m=-\ell}^{\ell} r^{\ell} A_{\ell}^{m} \left(Y_{\ell}^{-m} + (-1)^{m} Y_{\ell}^{m} \right) \qquad (2)$$

It is known from time-reversal invariance that ℓ is even ($\ell \leq S$). Therefore,

$$V(r\theta\phi) = \sum_{\ell=0}^{2S} \sum_{m=-\ell}^{\ell} r^{2\ell} A_{2\ell}^{m} \left(Y_{2\ell}^{-m} + (-1)^{m} Y_{2\ell}^{m} \right) \qquad (3)$$

A charge distribution produces a potential $V(r\theta\phi)$ for several electrons j which gives rise to the crystal field Hamiltonian[9]

$$\begin{aligned} H_{cf} &= e \sum_{j} V(r_j \theta_j \phi_j) \\ &= \sum_{k=0}^{2S} \sum_{q=-k}^{k} B_k^q O_k^q \end{aligned} \qquad (4)$$

where the $O_k^q = O_{2\ell}^m$ are operator equivalents to $r^{2\ell}$ ($Y_{2\ell}^{m}$ + + $(-1)^m Y_{2\ell}^m$). The number of terms in the expansion is limited by the electronic configuration of the transition ion which is interacting with the crystal field.

The interaction Hamiltonian[9] for the electronic spin S coupled to a nuclear spin I in a magnetic field H is

$$H = \beta_n \left(\bar{H} \cdot \bar{\bar{g}}_n \cdot \bar{I} \right) + \bar{S} \cdot \bar{\bar{A}} \cdot \bar{I} \qquad (5)$$

The first term is the nuclear Zeeman interaction where β_n is the nuclear magneton and g_n is the nuclear g-tensor. The second term is the hyperfine structure where $\bar{\bar{A}}$ is the hyperfine coupling tensor.

Thus the general interaction Hamiltonian[9] for an electronic spin S = 5/2 coupled to a nuclear spin I = 1/2 in a magnetic field H is

$$\mathcal{H} = \beta\,(\bar{H} \cdot \bar{\bar{g}} \cdot \bar{S}) + \sum_{\substack{-4=q=4 \\ k<4}} B_k^q O_k^q + \beta_n\,(\bar{H} \cdot \bar{\bar{g}}_n \cdot \bar{S}) + \bar{S} \cdot \bar{\bar{A}} \cdot \bar{I} \quad (6)$$

where the crystal field term expansion is

$$\mathcal{H}_{cf} = B_2^0 O_2^0 + B_2^1 O_2^1 + B_2^2 O_2^2 + B_4^0 O_4^0 + B_4^1 O_4^1 + B_4^2 O_4^2 + B_4^3 O_4^3 + B_4^4 O_4^4 + B_2^{-1} O_2^{-1} + B_2^{-2} O_2^{-2} + B_4^{-1} O_4^{-1} + B_4^{-2} O_4^{-2} + B_4^{-3} O_4^{-3} + B_4^{-4} O_4^{-4} \quad (7)$$

The matrix elements of the tensor operators O_k^q for S = 5/2 are tabulated in Ref. (8). The elements are diagonal for operators with q = 0 and off-diagonal for q ≠ 0.

The spin Hamiltonian may be further simplified for the ion under consideration from a knowledge of the point group symmetry of the site of the ion. The terms on the right hand side of Eq. (7) which do not conform to the point group symmetry are eliminated. The greater the point group symmetry the smaller will be the number of terms (hence the number of parameters) in the Hamiltonian. The point group symmetries and the spin Hamiltonian for each of the crystals investigated will be discussed in the following two sections.

2.1. Spin Hamiltonian For Fe^{3+} in Guanidinium Aluminum Sulfate Hexahydrate

The crystal structure of guanidinium aluminum sulfate hexahydrate (GASH) has been determined by Geller and Booth.[10] The unit cell parameters are : a = 11.745Å and c = 8.592 Å.[11] The point group symmetry of this trigonal crystal is C_{3v} and the space group is P_{31m} with three molecules per unit cell as shown in Fig. 2.1. The Al^{3+} ions (replaced by Fe^{3+}) are on a threefold axis and are surrounded by a somewhat distorted octahedra of water molecules. The guanidinium ions lie above and below the octahedra and are loosely bound indicating the possibility of disorder on rotation.[12] Of the three Al^{3+} (Fe^{3+}) ions per unit cell, two are equivalent to each other and belong to site II; the other belongs to site I. In the EPR spectra of Fe^{3+} in GASH this is equivalent to having two sets of spectra superimposed on each other, the intensities of the lines corresponding to site II being twice the intensities of the lines corresponding to site I.

The C_{3v} point group symmetry of GASH is consistent with the tensor operators O_2^0, O_4^0, O_4^3 and O_4^{-3}, thus the spin Hamiltonian as written by Bleaney and Trenam[13] for Fe^{3+} in GASH is

$$\mathcal{H} = \beta\,(\bar{H} \cdot \bar{\bar{g}} \cdot \bar{S}) + B_2^0 O_2^0 + B_4^0 O_4^0 + B_4^3 O_4^3 + B_4^{-3} O_4^{-3} \qquad (8)$$

The Hamiltonian is expressed with the Z-axis being parallel to the crystalline c-axis.

The explicit calculation of the elements of Eq. (8) leads to the following Hamiltonian matrix.

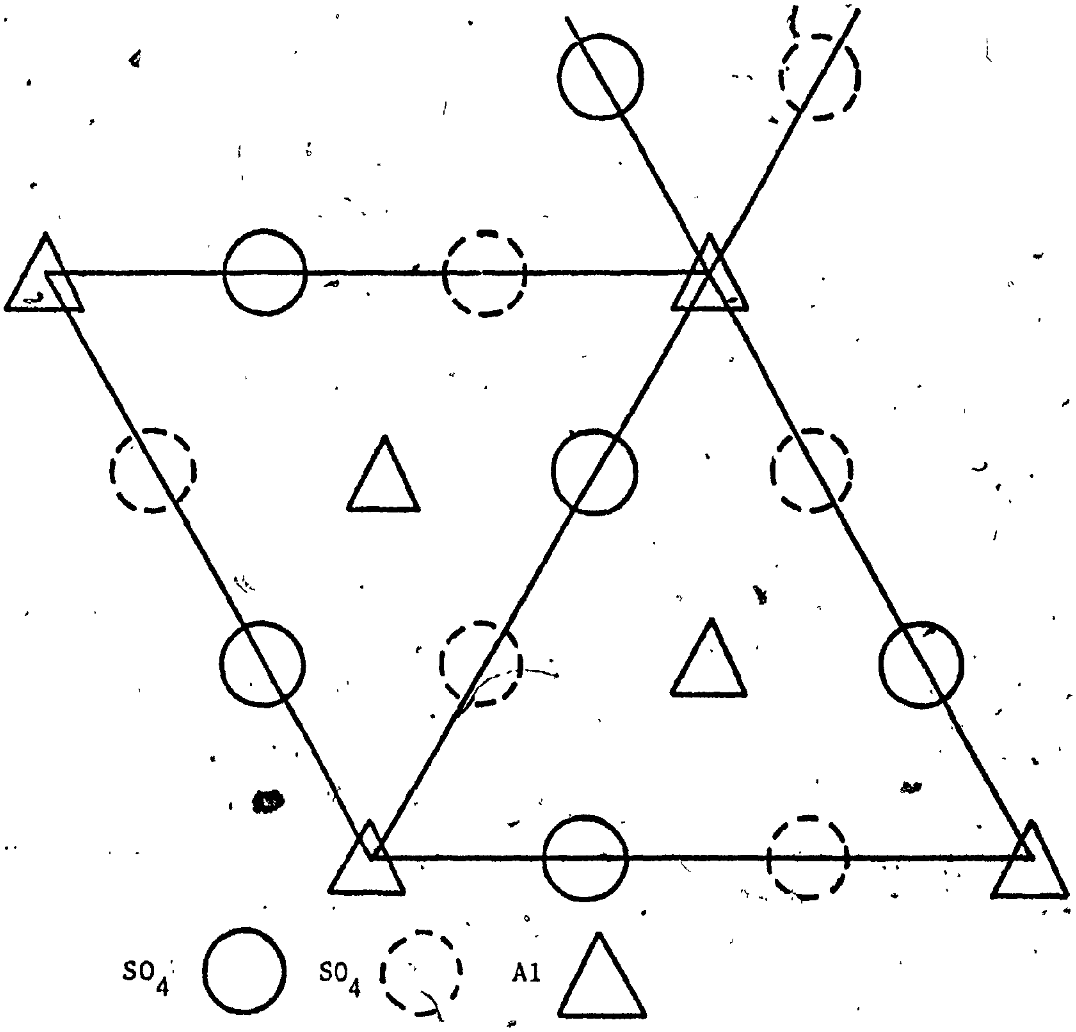

Fig. 2.1. A schematic of a unit cell of GASH looking down the c-axis. The triangles represent threefold axes with Al ions in the plane of the paper and a guanidinium ion above and below. Each Al ion is octahedrally surrounded by six waters. The circles represent SO_4^{--} groups above the plane and the dotted ones below.

	5/2	3/2	1/2	-1/2	-3/2	-5/2
5/2	$2.5\beta H(g_{zz}\cos\theta$ $+ g_{zx}\sin\theta)$ $+ 10B_2^0 + 60B_4^0$	$\sqrt{5/2}\beta H(g_{xx}\sin\theta$ $+ g_{zx}\cos\theta$ $- ig_{zx}\cos\theta)$		$3\sqrt{10}(B_4^3 - iB_4^{-3})$		
3/2	$\sqrt{5/2}\beta H(g_{xx}\sin\theta$ $+ g_{zx}\cos\theta$ $+ ig_{zx}\cos\theta)$	$1.5\beta H(g_{zz}\cos\theta$ $+ g_{zx}\sin\theta)$ $- 2B_2^0 - 180B_4^0$	$\sqrt{2}\beta H(g_{xx}\sin\theta$ $+ g_{zx}\cos\theta$ $- ig_{zx}\cos\theta)$			
1/2		$\sqrt{2}\beta H(g_{xx}\sin\theta$ $+ g_{zx}\cos\theta$ $+ ig_{zx}\cos\theta)$	$.5\beta H(g_{zz}\cos\theta$ $+ g_{zx}\sin\theta)$ $- 8B_2^0 + 120B_4^0$	$1.5\beta H(g_{xx}\sin\theta$ $+ g_{zx}\cos\theta$ $-ig_{zx}\cos\theta)$		$-3\sqrt{10}(B_4^3 + iB_4^{-3})$
-1/2	$3\sqrt{10}(B_4^3 + iB_4^{-3})$		$1.5\beta H(g_{xx}\sin\theta$ $+ g_{zx}\cos\theta$ $+ ig_{zx}\cos\theta)$	$-.5\beta H(g_{zz}\cos\theta$ $+ g_{zx}\sin\theta)$ $- 8B_2^0 + 120B_4^0$	$\sqrt{2}\beta H(g_{xx}\sin\theta$ $+ g_{zx}\cos\theta$ $-ig_{zx}\cos\theta)$	
-3/2				$\sqrt{2}\beta H(g_{xx}\sin\theta$ $+ g_{zx}\cos\theta$ $+ ig_{zx}\cos\theta)$	$-1.5\beta H(g_{zz}\cos\theta$ $+ g_{zx}\sin\theta)$ $- 2B_2^0 - 180B_4^0$	$\sqrt{5/2}\beta H(g_{xx}\sin\theta$ $+ g_{zx}\cos\theta$ $- ig_{zx}\cos\theta)$
-5/2			$-3\sqrt{10}(B_4^3 - iB_4^{-3})$		$\sqrt{5/2}\beta H(g_{xx}\sin\theta$ $+ g_{zx}\cos\theta$ $+ ig_{zx}\cos\theta)$	$-2.5\beta H(g_{zz}\cos\theta$ $+ g_{zx}\sin\theta)$ $+ 10B_2^0 + 60B_4^0$

Hamiltonian Matrix

2.2. Spin Hamiltonian For Fe^{3+} in Di-Ammonium Indium Pentachloride Monohydrate

The crystal structure of di-ammonium indium pentachloride monohydrate [$(NH_4)_2InCl_5 \cdot H_2O$] has been studied by X-ray diffraction methods,[14] as well as optical goniometry.[15] The dimensions of the unit cell are a = 14.10Å, b = 10.17Å and c = 7.16Å. The point group symmetry of this orthorombic crystal is D_{2h} and the space group is P_{nma}. The lattice is built up of NH_4^- ions and an octahedral complex $(InCl_5 \cdot H_2O)^{2-}$ ions where Fe^{3+} replaces In^{3+}. The octahedra are distorted because of the unequal size of the Cl^- ion and the H_2O molecule.

Figure 2.2 shows the unit cell of $(NH_4)_2InCl_5 \cdot H_2O$[14] looking down the b axis. Indium (Iron) is surrounded by five chlorine atoms and a water molecule at the center of the distorted octahedron. The water molecule is not distributed randomly but occupies a particular corner of the octahedra that lie on the symmetry planes in the cell. In the diagram the octahedra located on the symmetry plane at y = 0.25 are delineated with full lines while those on the y = 0.75 are given with dashed lines. The various chlorine atoms of one octahedron are designated by Roman numerals. Each chlorine IV stands for two chlorines at equal distances above and below the symmetry plane. The NH_4^- ions are surrounded by a distorted cube of six chlorine atoms and two water molecules. At the NH_4^- positions in the diagram there are

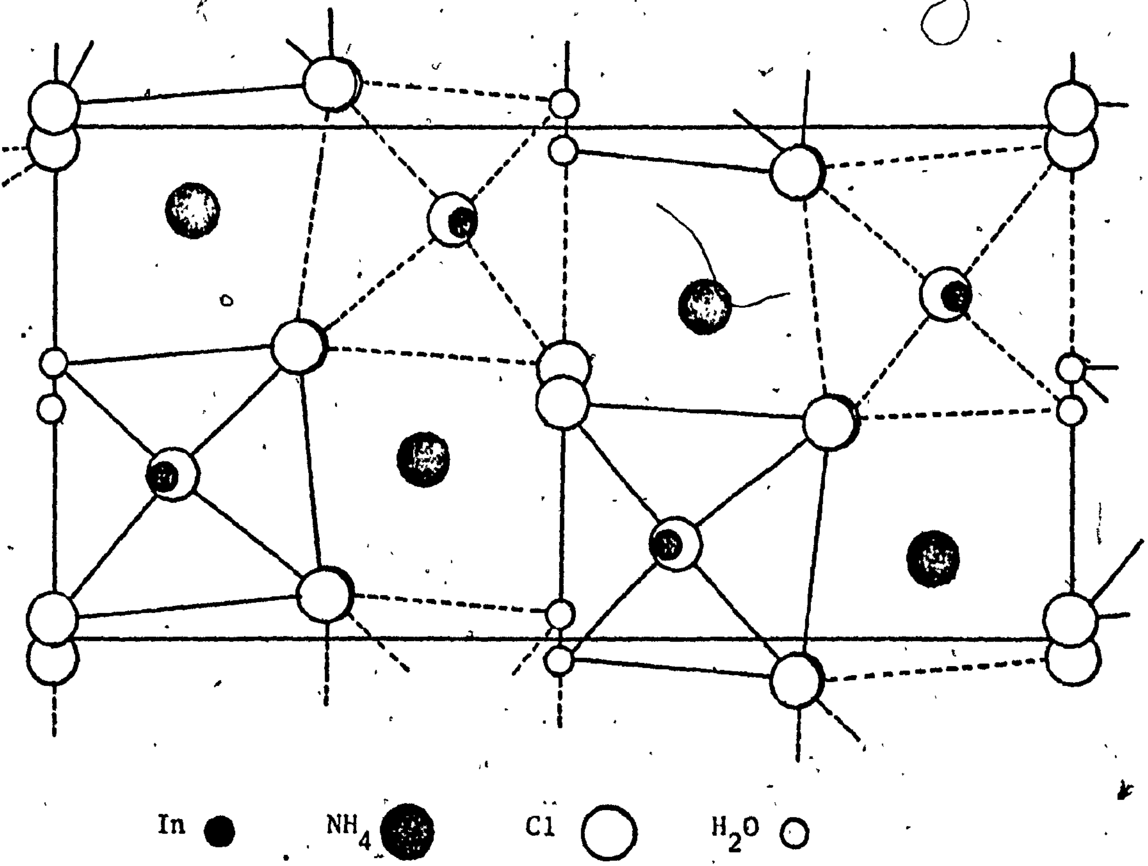

Fig. 2.2. A schematic diagram of a unit cell of $(NH_4)_2InCl_5\cdot H_2O$ looking down the b-axis.

actually two NH_4^- groups separated from each other by half the length of the b-axis.[14]

The unit cell contains four In^{3+} (Fe^{3+}) ions, labelled 1, 2, 3 and 4. Sites 1 and 4 form one magnetically equivalent pair as do sites 2 and 3. In the EPR spectra of Fe^{3+} in $(NH_4)_2InCl_5{\cdot}H_2O$ this is equivalent to having two identical sets of spectra superimposed on each other, the intensities if site I and site II being equal. It is noted that all four sites share a common b-axis thus the spectra along this axis will not be split due to the two sites.

The D_{2h} symmetry of the host lattice is consistent with the tensor operators O_2^0, O_2^2, O_4^0, O_4^2 and O_4^4. Thus the spin Hamiltonian[15] for Fe^{3+} in $(NH_4)_2InCl_5{\cdot}H_2O$ is given by

$$H = \beta \cdot (\overline{H} \cdot \overline{\overline{g}} \cdot \overline{S}) + B_2^0 O_2^0 + B_2^2 O_2^2 + B_4^0 O_4^0 + B_4^2 O_4^2 + B_4^4 O_4^4 \qquad (9)$$

Following the convention of Weger and Low[16] the axis along which the overall splitting of the lines is maximum is chosen to be the Z-axis. Of the two remaining axes, the axis along which the splitting is greater is chosen to be the X-axis of this coordinate system, the remaining axis is then the Y-axis. Unlike GASH the Z and Y-axes of the g-tensor do not coincide with any of the crystallographic axes, though they lie in the ac-plane of the crystal. The X-axis, however, coincides with the crystalline b-axis.

The explicit calculation of the elements of Eq. (9) leads to the following Hamiltonian matrix.

	5/2	3/2	1/2	-1/2	-3/2	-5/2
5/2	$2.5g_{zz}\beta H\cos\theta$ $+ 10B_2^0 + 60B_4^0$	$\sqrt{5/2}g_{xx}\beta H\sin\theta +$ $\sqrt{5/2}g_{yy}\beta Hi\sin\theta$	$\sqrt{10}B_2^2 + 9\sqrt{10}B_4^2$		$12\sqrt{5}B_4^4$	
3/2	$\sqrt{5/2}g_{xx}\beta H\sin\theta -$ $\sqrt{5/2}g_{yy}\beta Hi\sin\theta$	$1.5g_{zz}\beta H\cos\theta$ $- 2B_2^0 - 180B_4^0$	$\sqrt{2}g_{xx}\beta H\sin\theta +$ $\sqrt{2}g_{yy}\beta Hi\sin\theta$	$3\sqrt{2}B_2^2 - 15\sqrt{2}B_4^2$		$12\sqrt{5}B_4^4$
1/2	$\sqrt{10}B_2^2 + 9\sqrt{10}B_4^2$	$\sqrt{2}g_{xx}\beta H\sin\theta -$ $\sqrt{2}g_{yy}\beta Hi\sin\theta$	$.5g_{zz}\beta H\cos\theta$ $-8B_2^0 + 120B_4^0$	$3/2g_{xx}\beta H\sin\theta +$ $3/2g_{yy}\beta Hi\sin\theta$	$3\sqrt{2}B_2^2 - 15\sqrt{2}B_4^2$	
-1/2		$3\sqrt{2}B_2^2 - 15\sqrt{2}B_4^2$	$3/2g_{xx}\beta H\sin\theta -$ $3/2g_{yy}\beta Hi\sin\theta$	$-.5g_{zz}\beta H\cos\theta$ $- 8B_2^0 + 120B_4^0$	$\sqrt{2}g_{xx}\beta H\sin\theta +$ $\sqrt{2}g_{yy}\beta Hi\sin\theta$	$\sqrt{10}B_2^2 + 9\sqrt{10}B_4^2$
-3/2	$12\sqrt{5}B_4^4$		$3\sqrt{2}B_2^2 - 15\sqrt{2}B_4^2$	$\sqrt{2}g_{xx}\beta H\sin\theta -$ $\sqrt{2}g_{yy}\beta Hi\sin\theta$	$-1.5g_{zz}\beta H\cos\theta$ $- 2B_2^0 - 180B_4^0$	$\sqrt{5/2}g_{xx}\beta H\sin\theta +$ $\sqrt{5/2}g_{yy}\beta Hi\sin\theta$
-5/2		$12\sqrt{5}B_4^4$		$\sqrt{10}B_2^2 + 9\sqrt{10}B_4^2$	$\sqrt{5/2}g_{xx}\beta H\sin\theta -$ $\sqrt{5/2}g_{yy}\beta Hi\sin\theta$	$-2.5g_{zz}\beta H\cos\theta$ $+ 10B_2^0 + 60B_4^0$

Hamiltonian Matrix

2.3. Signs of Crystal Field Parameters

It is well known that each of the parameters g_{zz}, g_{xx} and g_{yy} are positive, however, the absolute signs of the various B_k^q must be determined using the intensities of the lines at low temperature. In order to uniquely determine the signs of all the parameters one only needs to determine the signs of one of the B_k^q with q even, since their relative signs can be determined from the EPR data at any temperature. As in the discussion of Abragam and Bleaney,[8] the most appropriate parameter for this purpose is B_2^0, the parameter that determines the zero field splitting. Then at low temperature, since (i) the intensities of lines are proportional to the population differences between the levels which the resonance takes place, (ii) the greater the population of a level the lower is its energy, thus B_2^0 is positive (negative) if the observed intensity of $|\Delta M| = 1$ (M are the magnetic quantum numbers) lines which occur at the higher magnetic field are greater (smaller) than the intensities of the lines which occur at lower magnetic field values.

Therefore the energy difference between adjacent levels lying at a higher energy (differing in their magnetic quantum numbers by 1) is smaller than that between adjacent levels lying at lower energy for B_2^0 greater than zero; for B_2^0 less than zero the opposite is true. Once the signs of the parameters are determined, the lines may be identified with the correct quantum numbers.

CHAPTER III

EXPERIMENTAL APPARATUS

A reflection cavity X-band spectrometer[17] suitable for variable temperature measurements is used in making all the field dependent spin resonance measurements. A block diagram of the spectrometer is shown in Fig. 3.1. The description of the various components is as follows.

3.1. The Microwave Spectrometer

The microwave source is a forced air cooled Varian X-13 reflex klystron with a frequency range of 8.1 to 12.4 gHz and a power rating of 180 m . A Hewlett Packard model 715A power supply produces the required beam voltage of +400 Vdc with a ripple of less than 7 mV and a beam current of 50 mA. A range of reflector voltages from 0 to -900 Vdc with respect to the beam supply are available with a ripple of less than 10 mV. The filament voltage supply provides 1.5 Amps at 6.3 Vac.

Electronic control of the klystron operating frequency is acheived by a Micro-Now model 210 frequency stabilizer. The klystron frequency is stabilized by locking

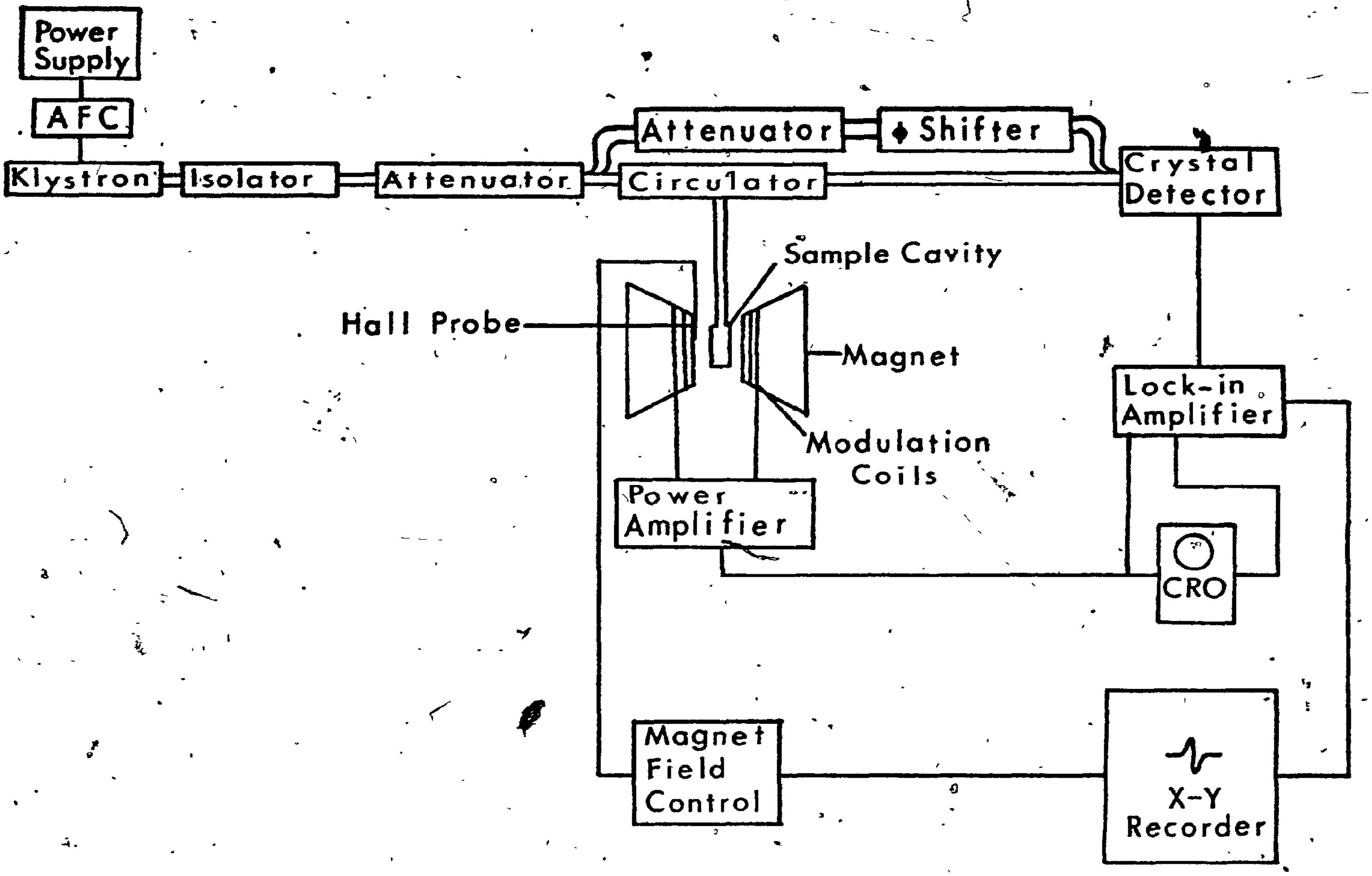

Fig. 3.1. Block diagram of the X-band spectrometer.

it to the resonant frequency of the sample cavity (rather than to an external reference cavity), so that if for any reason, such as small temperature changes of the sample cavity, which will change its resonant frequency, the klystron frequency will follow the change. Stabilization is achieved by applying a 10 kHz sine wave modulation voltage and a dc correction voltage in series with the klystron reflector voltage.

In the microwave bridge a three terminal E-M Laboratories model X112LY ferrite circulator is employed, which when compared to the case with a magic T, eliminates the division of incident power between the sample arm and the tuning arm of the spectrometer.[18]

A Hewlett Packard model 382 calibrated attenuator is connected between the load and the klystron to reduce the signal intensity incident upon the load. This is adjusted to give optimum signal to noise ratio. Proper biasing of the BAV 46 Schottky diode is provided by coupling off ten percent of the incident power into a bucking arm provided with an attenuator and a phase shifter. This power is coupled into the detecting arm after the circulator and is used to buck out or enhance the power incident on the diode detector.[7]

Figure 3.2 shows a detailed view of the cavity arm[19] of the spectrometer. Since this arm is designed for use inside the cryostat the top flange is sealed off for evacuation purposes by means of a mica sheet. The cavity arm is evacuated in order

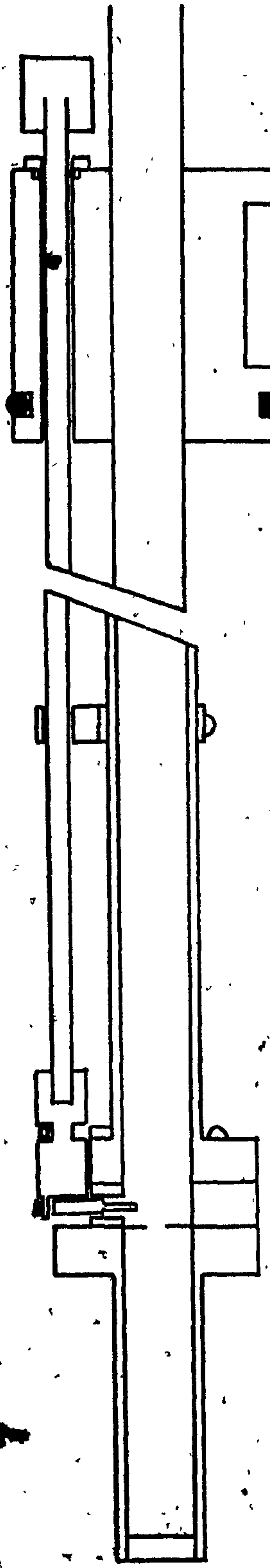

Fig. 3.2. Detailed view of cavity arm.

to reduce condensation which will otherwise disturb the tuning of the sample cavity at low temperatures.

The cavity, which is gold plated, is a rectangular type, resonating in the TE_{102} mode at a frequency of approximately 9.41 gHz at room temperature. The cavity is coupled to the waveguide by a 0.010 inch thick gold plated brass sheet with an iris in the center of 0.20 inch diameter. The cavity is matched to the waveguide by a 0.030 inch inductive pin. The pin is connected to a cam and rod which leads to the upper flange of the waveguide.

The resonant frequency of the microwave cavity is measured by observing the resonant magnetic field value for diphenyl picryl hydrazl (d.p.p.h.) for which $g = 2.0036 \pm .0002$. The peak-to-peak line-width of d.p.p.h. is measured to be .85 gauss which gives a possible error of approximately .025 percent in the calculation of the resonant frequency of the sample cavity. The resonant magnetic field is measured by a nuclear magnetic resonance fluxmeter which is discussed in section 3.3.

3.2. The Detecting and Amplifying Network

The magnetic field is modulated at a frequency of 520 Hz which is internally produced by the lock-in-amplifier. To obtain the desired amplitude of the modulation field a power amplifier capable of producing 100 W rms and a maximum current of 7 Amps ac rms is employed. The modulation amplitude is adjusted to give a good representation of the desired derivatives of absorption curves.

The field modulation coils are wrapped on masonite forms and rigidly mounted on the magnet pole pieces. Each coil is 90 turns of number 12 insulated copper wire embedded in varnish. This is done in order to reduce the vibrations of the coils at large magnetic fields.

The crystal detector demodulates the microwave power which is transferred by coaxial cable to a Princeton Applied Research model 122 lock-in-amplifier. This instrument enables the rms value of the fundamental frequency (520 Hz) component to be measured accurately.

The resulting dc output from the lock-in-amplifier is plotted on a Moseley model 7005-A servo-potentiometer X-Y recorder. The X-axis is driven by a fraction of the signal provided by the "X-axis drive" of the Varian Fieldial which is used to regulate and sweep the magnetic field. The Y-axis is driven by the output of the lock-in-amplifier, thus yielding a plot of the derivative of absorption versus magnetic field.

3.3. The Magnetic Field and its Measurement

The magnetic field is provided by a Varian model V-3900 electromagnet capable of producing a field of 13 kG across a 3-inch magnet gap. The Varian 10 kw, model VFR-2803 Control unit has digital field controls with increments of 0.10 Gauss. Sweep ranges from 0.25 G to 25 kG with sweep times of 0.50 min to 100 min can be selected. A temperature controlled Hall-Effect crystal probe mounted on a magnet pole cap maintains the magnetic field within one percent of the selected field value.

The digital field controls were calibrated by means of nuclear magnetic resonance probes containing protons for fields of 1 kG to 8 kG and deutrons for fields from 8 kG to 13 kG. The difference between the fieldial reading and the true magnetic field is found to be linear over the range from 1 kG to 13 kG. As no accurate measuring device is available for fields less than 1 kG, in this region the field is estimated assuming that the field is linear. The instrument used to make field measurements is a Varian model F-8 nuclear fluxmeter and a Hewlett Packard model 5245-N frequency counter. Neglecting inhomogeneities in the magnetic field the possible error in magnetic field is .0028 percent throughout the range of the fluxmeter.

For the experiments performed at room and nitrogen temperatures each magnetic resonance line observed is measured by the nuclear fluxmeter to provide greatest possible accuracy. For fields below 1 kG the chart recorder output is calibrated using measured magnetic fields extrapolated to include lines of interest. For helium temperature, due to restricted length of time for an experiment the magnetic fields are measured along the principal axes of the crystal using the nuclear fluxmeter for each resonant line. The magnetic fields at intermediate angles are measured using a calibration curve.

3.4. Low Temperature Apparatus and Temperature Measurement

The totally metallic variable temperature cryostat, similar to many commercially available, was constructed in the workshop specifically for the detection of dynamically oriented nuclei and is fully described in Ref. (20). The main feature of the cryostat is windows in the tail section which allow for irradiation of a sample located inside the microwave cavity.

The temperature is controlled by an Artronix model 5301 temperature controller capable of control over a range of 1.0 K to 320 K. Two temperature sensors are mounted in the brass flange above the sample cavity. A germanium resistor is calibrated from 1.5 K to 37.1 K with an error of .95 percent and a platinum resistor from 30.0 K to 102.4 K with an error of 0.75 percent. The temperature is controlled by a 100 ohm double-silked manganin wire heater wrapped around the cavity; up to 25 W rms can be generated.

CHAPTER IV

PROCEDURE FOR THE ANALYSIS OF DATA

With the knowledge of the spin Hamiltonian and the observed magnetic resonance transitions the spin Hamiltonian parameters can be evaluated. These parameters are useful in calculations of dynamic nuclear orientation and the analysis of Mossbauer data.

The usual method of analysis employs perturbation theory, applicable provided that the off-diagonal terms in the spin Hamiltonian are sufficiently small. Moreover, it is incapable of determining the off-diagonal elements separately. Better methods of analysis are those which utilize exact computer diagonalization, e.g. the method of Buckmaster et. al.[21] which is applicable when the off-diagonal terms are small. Methods capable of yielding more accurate individual parameters have been described by Misra and Sharp,[22] and Misra.[5]

The method developed by Misra and Sharp[22] is a brute-force method, in that no mathematical criteria are used to alter the values of the parameters so as to yield a minimum "chi-squared". The method of Misra utilizes the least-square fitting procedure. The main features common to both methods are simultaneous consideration of resonant magnetic field values corresponding to (i) more than one orientation of the magnetic field (ii) if required, consideration of resonant magnetic field values corresponding to $\Delta M > 1$ transitions (M is the magnetic quantum number), in addition to those corresponding to $\Delta M = 1$ transitions.

4.1. Brute-Force Method

In this section the details of the brute-force method of Misra and Sharp[22] are described. One is concerned with the evaluation of the parameters g_{ij} and B_k^q of the spin Hamiltonian. All B_k^q of the same k value have the same order of magnitude as they transform among themselves under the transformation of coordinate axes. Thus, in this method the parameters belonging to the same angular momentum value k are varied simultaneously until the lowest $\mathrm{SMD} \equiv \sum_{jk} (|\Delta E_{jk}| - h\nu)^2$ in the variation range is obtained. Here ν is the microwave frequency, h is Planck's constant, $\Delta E_{jk} = E_j - E_k$; E_j and E_k are the energies of levels between which the microwave energy is being absorbed at resonance.

The various subgroups in descending order of magnitude are usually $\{g_{ij}\}$, $\{B_2^q\}$, $\{B_4^q\}$, etc. where { } denotes a subgroup, where this is not the case, the appropriate ordering in subgroups of same angular momentum value in descending order of magnitude is chosen. When considering the resonant magnetic field values corresponding to the magnetic field orientation being parallel to one of the principal axes of the g-tensor, one has only to vary the corresponding g-value since the g-values in the other directions do not contribute to the spin Hamiltonian.

The various steps in the computation procedure of the brute-force method are as follows:

(a) Choose appropriate resonant magnetic field values corresponding to two or more orientations of the static magnetic field. One needs at least as many resonant magnetic field values as there are parameters, the larger the number of magnetic field values used for computation the more realistic will be the values of the parameters obtained.

(b) Choose the initial values of the parameters and their ranges over which they are to be varied. Some parameters may be estimated by means of perturbation theory or by considering only the diagonal terms of the spin Hamiltonian. Usually the same ranges of parameters may be chosen for the B_k^q characterized by the same k value.

(c) Arrange the subgroups of the parameters in descending order of magnitudes of their values (i.e. in the order of increasing k) . The parameters are given values about their initial values in the following manner.

$$B_k^q = B_k^q \text{(initial)} + n\Delta B_k^q$$

where n = -m, -(m-1),...0,...(m-1), m: m is an appropriate chosen integer depending upon the computer time available, and ΔB_k^q is the increment in the value of B_k^q in each step. Thus, for example, for M = 2 five values are available, two being less and two being greater than the initial value.

(d) In each iteration in the computation the various parameters are considered in subgroups starting with the term having the smallest angular momentum, i.e., with g_{xx}, g_{yy}, and g_{zz} (these are parameters of the type B_1^q, being the coefficients of S_x, S_y and S_z respectively in the spin Hamiltonian) and then consider the other subgroups in order of increasing k. While considering a subgroup all the possible combinations of the values of the parameters in that subgroup available in the ranges are considered. Of these, the one that yields the lowest SMD is retained to serve as the initial set of values for that subgroup in the next iteration, as well as for variation of parameters in other subgroups with higher k in the iteration. The particular set of all the parameters in any iteration which yields the lowest SMD (this is referred to hereafter as SMD_{min}) thus determined is used as the set of initial values for the next iteration. This SMD_{min} is now compared with an initially chosen small value V_{min} consistent with experimental uncertainties. In the next iteration, the searching ranges of the parameters are reduced (which is equivalent to reducing ΔB_k^q) by an appropriate factor f. In order to ensure adequate overlap of values of parameters between succesive iterations f should be less than or equal m. As before the values of parameters corresponding to the SMD_{min} are found by varying the values of parameters over their ranges, considering them in subgroups. If SMD_{min} is less than or equal V_{min}, the computation is complete, otherwise successive iterations are done until SMD_{min} is less than or equal to V_{min}.

Gd^{3+} (S = 7/2) in $SmCl_3 \cdot 6H_2O$ [23] has been analyzed by the brute-force method using magnetic resonance transitions along the Z and X-axes of the principal axis system at an X-band frequency. The results obtained using this method, the method of Buckmaster et. al.[21] second and fourth-order perturbation approaches are listed in Table 4.1. From the SMD values obtained using the various methods of analysis it can be seen that the brute-force method yields the more accurate values of parameters.

Table 4.1. Values of parameters (gHz) yielding the lowest SMD (gHz^2) possible, for the various methods used.

Parameter	Second-order Perturbation Theory	Fourth-order Perturbation Theory	Buck-master et. al.	Brute Force Method
g_{zz}	1.98580	1.97573	1.98502	1.99132
g_{xx}	1.99649	1.91625	1.97060	1.99230
b_2^0	1.85589	1.82749	1.85413	1.87065
b_2^2	-1.05178	-0.77682	-1.03042	-1.11419
b_4^0	-0.02905	-0.02397	-0.02953	-0.03311
b_4^2	-	-	0.01016	0.02837
b_4^4	-	-	0.00469	0.00109
b_6^0	-0.00204	-0.00217	-0.00064	0.00108
b_6^2	-	-	-0.00664	0.02875
b_6^4	-	-	-0.03148	0.02906
b_6^6	-	-	-0.00742	0.01594
SMD	0.2703	0.8753	0.4537	3.10×10^{-4}

The initial values of parameters used for the brute-force procedure are: g_{zz}, g_{xx}, b_2^0, b_2^2, b_4^0, and b_6^0 those determined by second-order perturbation theory listed in Table 4.1 and b_4^2, b_4^4, b_6^2, b_6^4 and b_6^6 are taken to be zero. The incremental values per step for the various parameters were chosen to be $\Delta g_{zz} = \Delta g_{xx} = .01$, $\Delta b_2^q = .05$ gHz (q = 0, 2), $b_4^q = 0.5$ gHz (q = 0, 2, 4), $b_6^q = 0.05$ gHz (q = 0, 2, 4, 6). Thirteen resonant magnetic field values for X-band (six along Z and seven along X) are simultaneously considered for the evaluation of the parameters. The results of the computation of the parameters are summarized in APPENDIX I (the incremental values per step are changed after the seventh iteration).

The advantages of this method over the perturbation approach are that all the individual values of parameters are calculated rather than linear combinations of some of the parameters. Furthermore, it contains orthogonal-axis consistency unlike the method of Buckmaster et. al. In the latter method a set of parameters may be obtained which yields an extremely small SMD along one axis but does not yield an acceptable SMD for resonant magnetic fields in a direction perpendicular to it.

One difficulty with the brute-force method is the amount of computer time required to analyze the data. For the thirteen lines analyzed for Gd^{3+} in $SmCl_3 \cdot 6H_2O$, 160 minutes of computer time on the CDC 6400 were required. This shortcoming, however is overcome by using a least-squares fitting procedure developed by Misra.

4.1.1. Least-Squares Fitting Procedure

In this method considerably less computer time is required to analyze the data since the values of the parameters corresponding to the absolute minimum "chi-squared" value are obtained using mathematical criteria of the method of least-squares.[5] The inability to write down the derivatives is here circumvented by using numerical techniques to compute the derivatives exactly. For the case of Gd^{3+} in $SmCl_3 \cdot 6H_2O$ the computing time is reduced to 2.4 minutes, a reduction of 68 times as compared to that required for the brute force method of Misra and Sharp. This method has been used to analyze a number of rare earth samples (see Refs. 24-28), and is also used to analyze the data for Fe^{3+} in GASH and $(NH_4)_2InCl_5 \cdot H_2O$ simultaneously fitting approximately 45 resonant magnetic field values along various directions.

The function S' (chi-squared) for EPR is

$$S' = \sum_{jk} \frac{(|\Delta E_{jk}| - h\nu)^2}{\sigma_i^2} \tag{10}$$

where σ_i is the weight factor (related to the standard deviation).

The vector $\vec{a}^m$ with components a_1^m, a_2^m, ...a_n^m describing the set of n parameters corresponding to the absolute minimum value of chi-squared, can be obtained from the vector $\vec{a}^I$

describing the initially chosen values of the parameters, from the equation

$$\vec{a}^{m} = \vec{a}^{I} - (D'')^{-1} D' \tag{11}$$

where D' is a column vector whose elements are first derivatives of S' with respect to the parameters evaluated at $\vec{a}^{I}$ and D'' is the matrix where the elements are the second derivatives with respect to the parameters evaluated at $\vec{a}^{m}$. Thus

$$D'_{k} = \left(\frac{\partial S'}{\partial a_{k}}\right)_{\vec{a}^{I}} \tag{12}$$

$$D''_{k_1 k_2} = \left(\frac{\partial^2 S'}{\partial a_{k_1}\, \partial a_{k_2}}\right)_{\vec{a}^{m}} \tag{13}$$

Since one does not know the $\vec{a}^{m}$ to begin with the elements of the matrix D'' are evaluated with respect to $\vec{a}^{I}$ (referred to as $D''(\vec{a}^{I})$); then one obtains a new set of parameters described by the vector $\vec{a}^{f}$, where

$$\vec{a}^{f} = \vec{a}^{I} - (D''(\vec{a}^{I}))^{-1} D' \tag{14}$$

in place of equation (11). Equation (14) is then used iteratively until a sufficiently small S' consistent with experimental uncertainties is obtained.

From equation (10) the derivatives are given by

$$\frac{\partial S'}{\partial a_j} = 2 \sum_i \frac{\Delta E_i}{|\Delta E_i|} \frac{(|\Delta E_i| - h\nu)}{\sigma_i^2} \left(\frac{\partial E_{i'}}{\partial a_j} - \frac{\partial E_{i''}}{\partial a_j}\right) \tag{15}$$

$$\frac{\partial S'}{\partial a_j \partial a_\ell} = 2\sum_i \frac{1}{\sigma_i^2}\left[\left(\frac{\partial E_{i'}}{\partial a_j} - \frac{\partial E_{i''}}{\partial a_j}\right)\left(\frac{\partial E_{i'}}{\partial a_\ell} - \frac{\partial E_{i''}}{\partial a_\ell}\right) + \right.$$

$$\left. + \frac{\Delta E_i}{|\Delta E_i|} \left(|\Delta E_i| - h\nu\right)\left(\frac{\partial^2 E_{i'}}{\partial a_j \partial a_\ell} - \frac{\partial^2 E_{i''}}{\partial a_j \partial a_\ell}\right)\right] \qquad (16)$$

where the a_j, constitute the components of vector $\vec{a}$ and stand for the parameters g_{ij} and B_k^q.

The method of evaluation of the first and second derivatives of $E_{i'}$ and $E_{i''}$ with respect to the parameters is performed by the application of Feynman's theorem and is outlined in Ref.

The least-squares fitting procedure applied to Gd^{3+} in $SmCl_3 \cdot 6H_2O$ yields the following parameters;

$g_{zz} = 1.9911$, $g_{xx} = 1.9923$, $b_2^0 = 1.8703$

$b_2^2 = -1.1142$, $b_4^0 = -0.0331$, $b_4^2 = 0.0288$

$b_4^4 = 0.0010$, $b_6^0 = 0.0011$, $b_6^2 = 0.0300$

$b_6^4 = 0.0309$, $b_6^6 = 0.0176$

$S' = 0.00030$

Comparing the least-squares fitting procedure with the brute-force method, it is seen that the values of parameters are equivalent within the limits of experimental error.

CHAPTER V

EXPERIMENTAL DETAILS AND ANALYSIS OF THE DATA FOR Fe^{3+} IN GASH

The crystals were grown from an aqueous solution of calculated amounts of guanidinium sulfate, aluminum sulfate and ferric sulfate. It was observed in Ref. (3) that the concentration of the iron relative to the aluminum was about a tenth of the starting ratio. The solution was made slightly acidic in order to prevent hydrolysis of the ferric ion, and was allowed to slowly evaporate from a partially covered beaker at room temperature. Small platelets first formed on the surface and then sank to the bottom of the solution where they were allowed to grow to sizes compatable with X-band cavity dimensions (approximately 5 mm in width by 2 mm thick).

The crystals grew in hexagonal plates as shown in Fig. 5.1, with normals accurately parallel to the crystal c-axis. For EPR measurements with the constant magnetic field in the plane perpendicular to the c-axis (XY plane), the crystal is placed flat on the bottom of the cavity with the c-axis pointing upwards. The crystal is placed at $\lambda_g/4$ (λ_g is the guide wavelength) from the top of the cavity with one edge of the crystal parallel to the bottom of the cavity for measurements in a plane containing the c-axis (ZX plane).

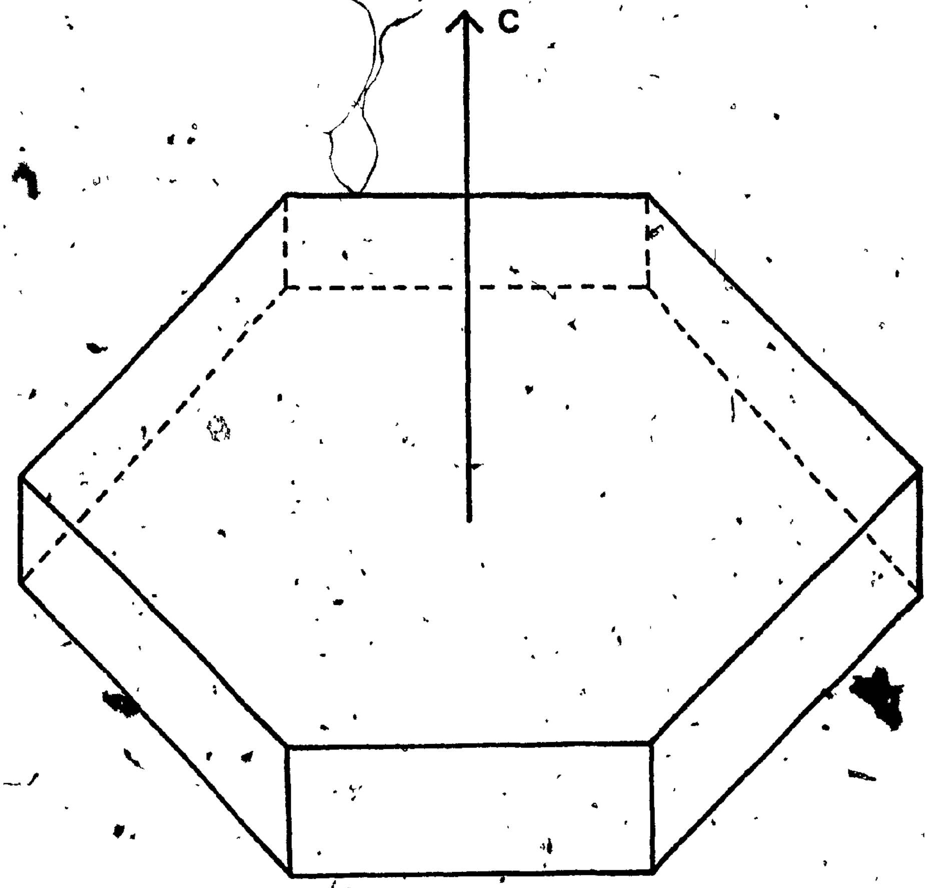

Fig. 5.1. Crystal growing habit of guanidinium aluminum sulfate hexahydrate.

5.1.1: Spectrum at 295 K

The spectrum was investigated for both sites I and II in the XY plane and was found to be invariant for the magnetic field orientation anywhere in the plane as shown in Fig. 5.2. It can easily be seen that this symmetry conforms with Eq. (8). The terms containing O_2^0 and O_4^0 are axially symmetric and the terms containing O_4^3 and O_4^{-3} have no effect on the observed spectra since the expectation values of the operators O_4^3 and O_4^{-3} are zero in a plane perpendicular to the c-axis. This spectrum also implies that $g_{xx} = g_{yy}$ and $g_{xy} = 0$. No numerical analysis of this data was performed as the same transitions are observed along the X-axis when the crystal is mounted in the ZX plane.

With the static magnetic field directed along the Z-axis (see Fig. 5.3) a total of fifteen lines are observed, seven belonging to site I and seven belonging to site II. The single line appearing at 3352 Gauss is the 1/2 ↔ -1/2 transition for both sites and is unsplit since the g values for each site are almost identical. With the static magnetic field along the X-axis (see Fig. 5.4) a total of four lines are observed, two unsplit lines which are common to both sites and a high field doublet, one line belonging to each site.

The angular variation of the spectra belonging to site I in the ZX plane is illustrated in Fig. 5.5. The spectra

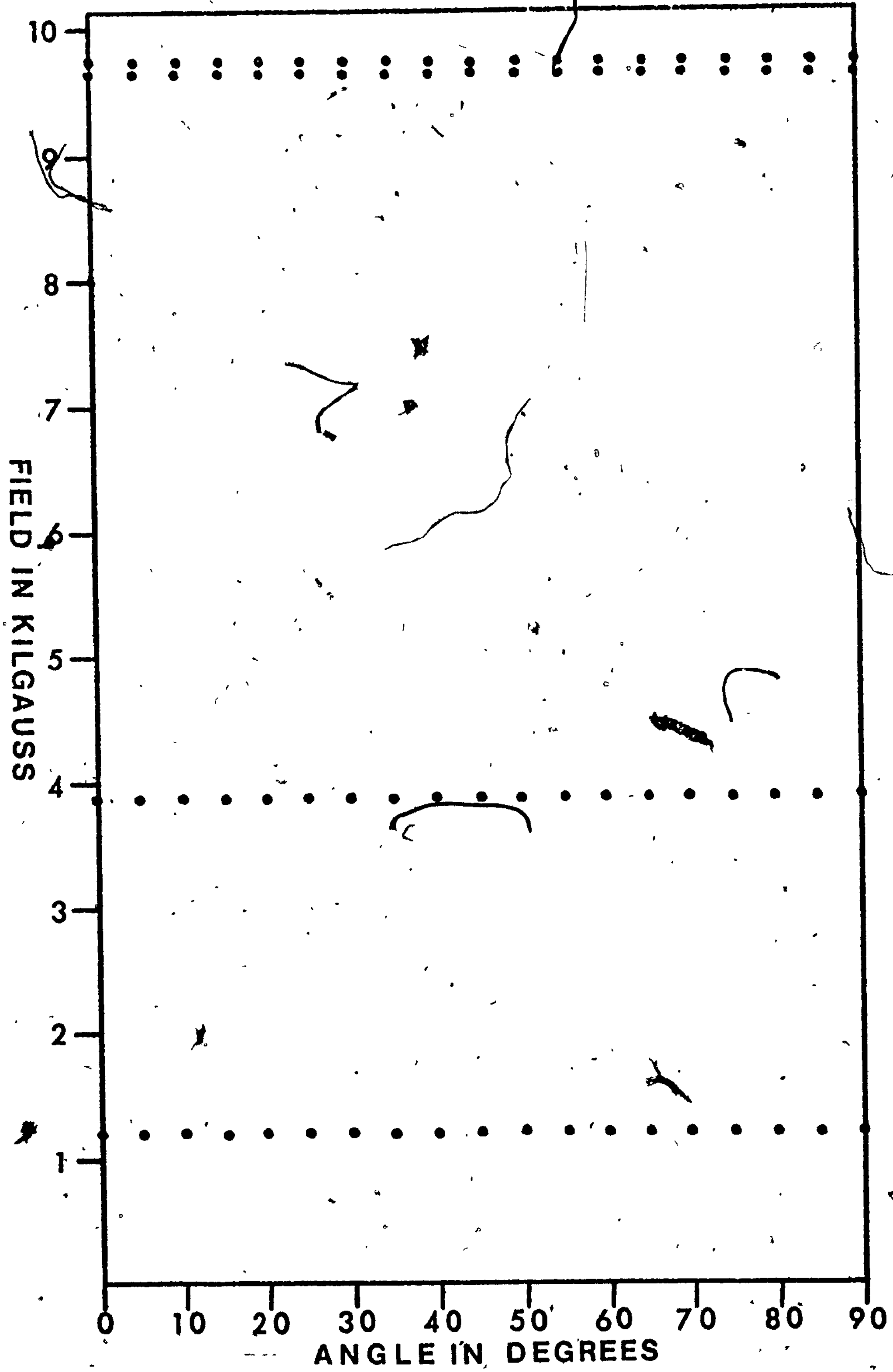

Fig. 5.2. The spectral angular variation for the static magnetic field in the XY plane.

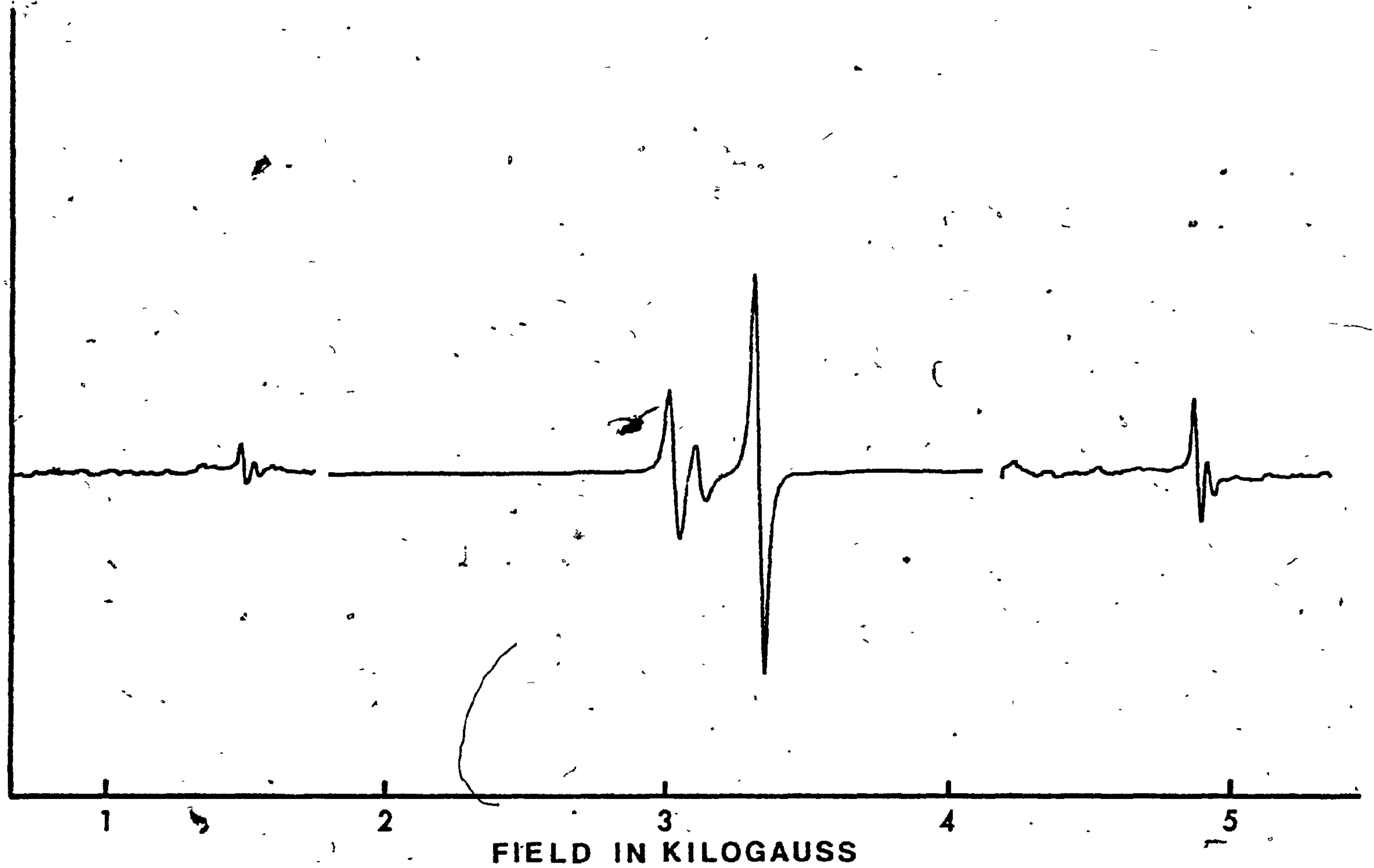

Fig. 5.3a EPR absorption spectrum with the static magnetic field directed along the Z-axis.

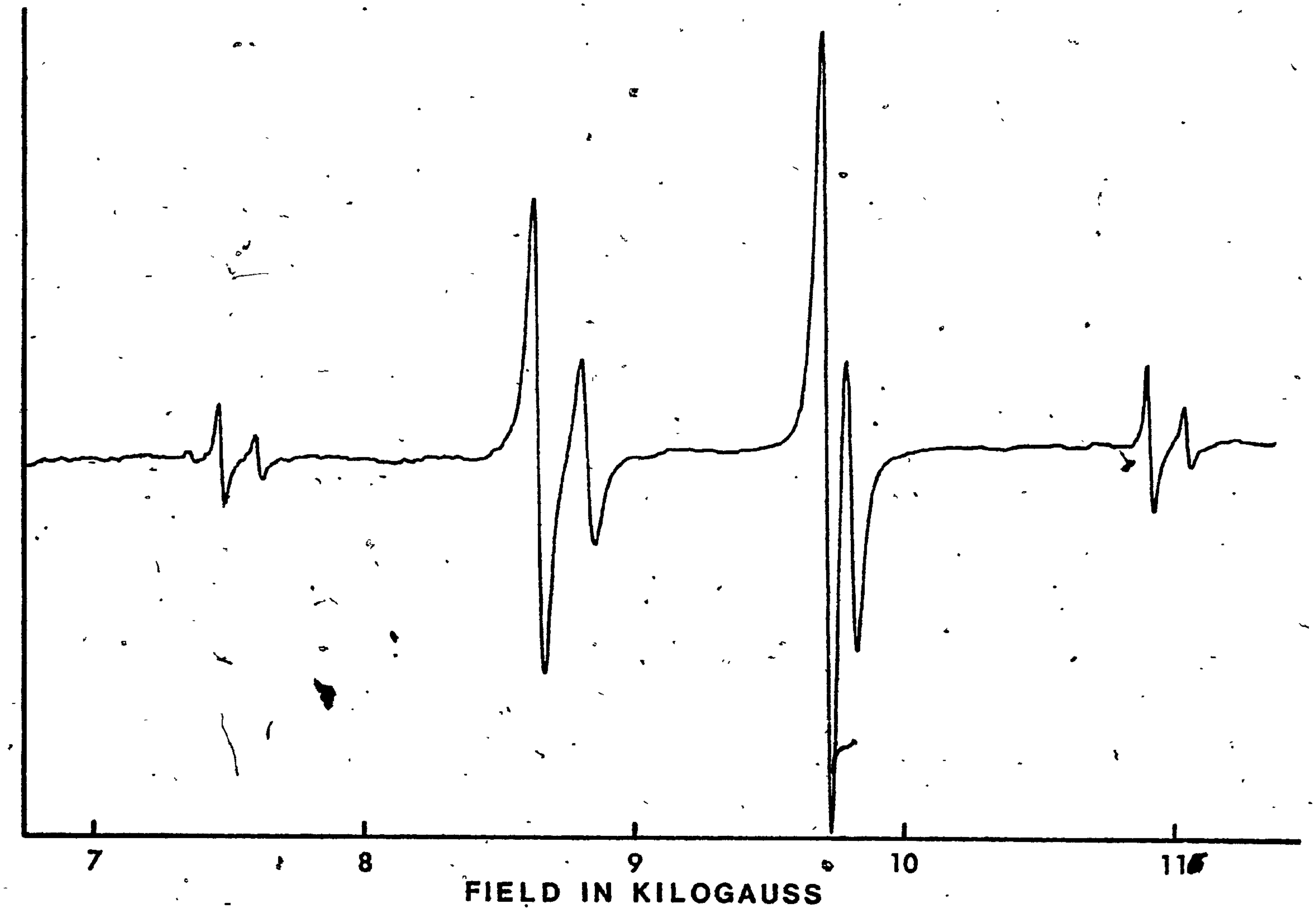

Fig. 5.3b EPR absorption spectrum with the static magnetic field directed along the Z-axis.

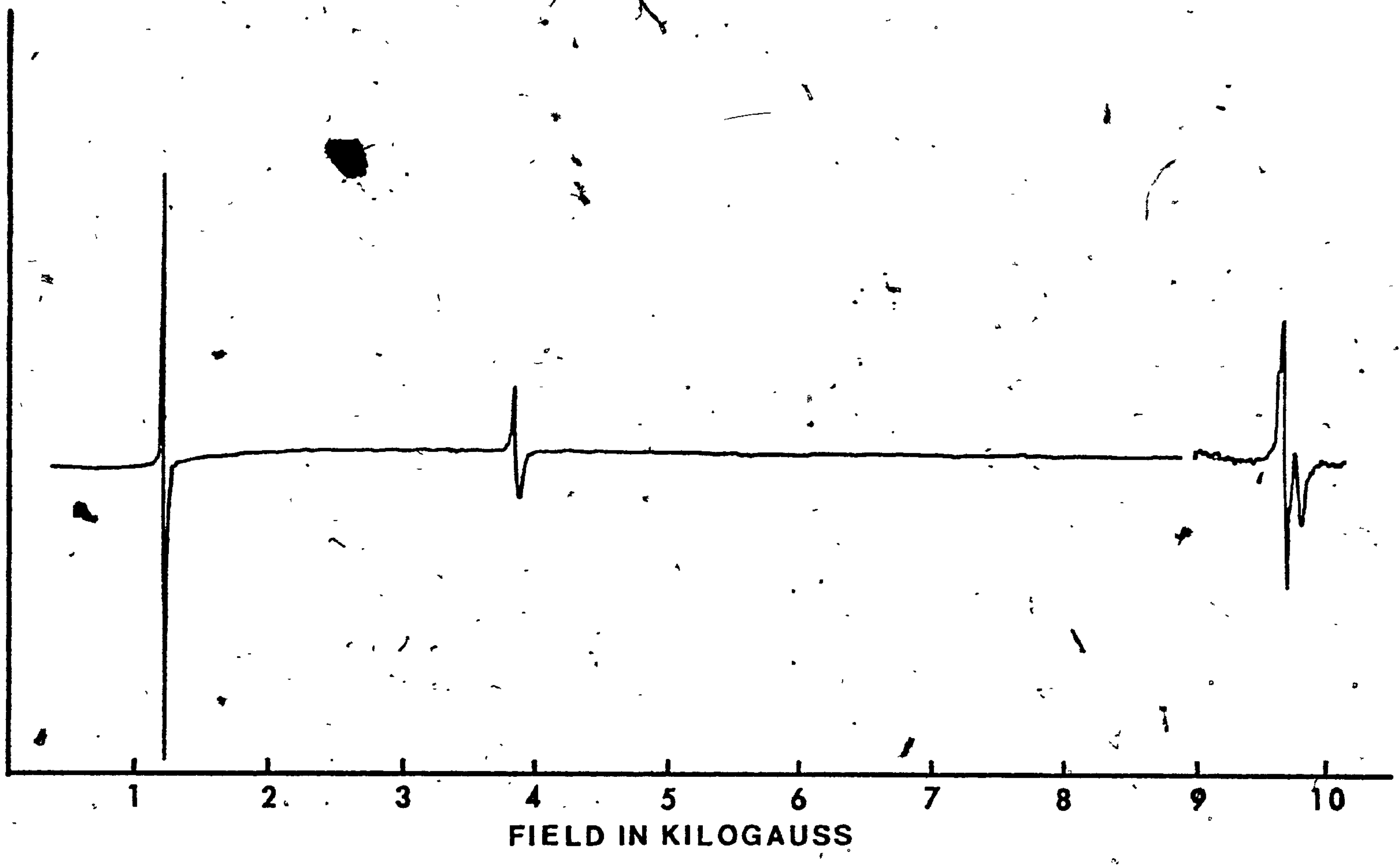

Fig. 5.4. EPR absorption spectrum with the static magnetic field directed along the X-axis.

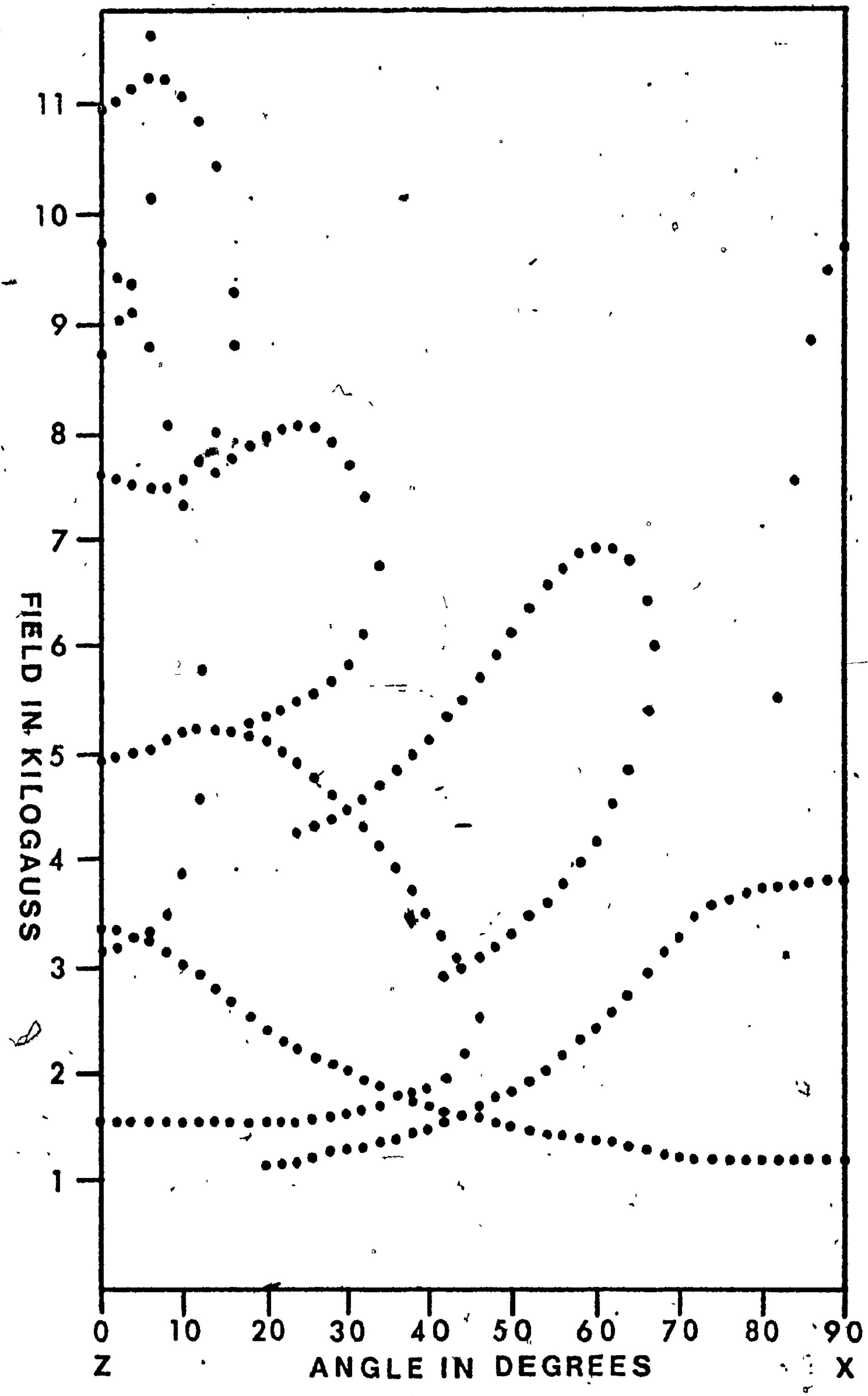

Fig. 5.5. Angular variation of the spectra belonging to site I in the ZX plane.

corresponding to site II lie at a slightly lower magnetic field and exhibit the same symmetry. Each site I line has half the intensity of the corresponding site II line.

The angular variation reveals that along the Z-axis there are two lines corresponding to the same transition for each of site I and site II. This is due to the fact that the energy eigenvalue equations have two solutions. Typically two lines are separated by several kilogauss along the Z-axis and merge into a single line at some angle from the Z-axis. This effect and the splitting of the two sites is well illustrated for the 5/2 ↔ 1/2 transition in Fig. 5.6.

The data for site I along the Z-axis was first analyzed using only the diagonal terms of the spin Hamiltonian

$$\mathcal{H} = \beta H g_{zz} S_z + B_2^0 O_2^0 + B_4^0 O_4^0 \quad , \qquad (17)$$

requiring only to solve three simultaneous equations.

Using the identification of transitions along the Z-axis reported in Ref. (3) the following data was used to calculate the parameters.

Transition	Magnetic Field (Gauss)
5/2 ↔ 3/2	10964
3/2 ↔ 1/2	9813
1/2 ↔ -1/2	3352

Using this set of parameters all the magnetic fields for $|\Delta M| = 1$, 2, 3, 4, 5 lines were calculated. It is found however that the parameters did not account for all the experimentally observed

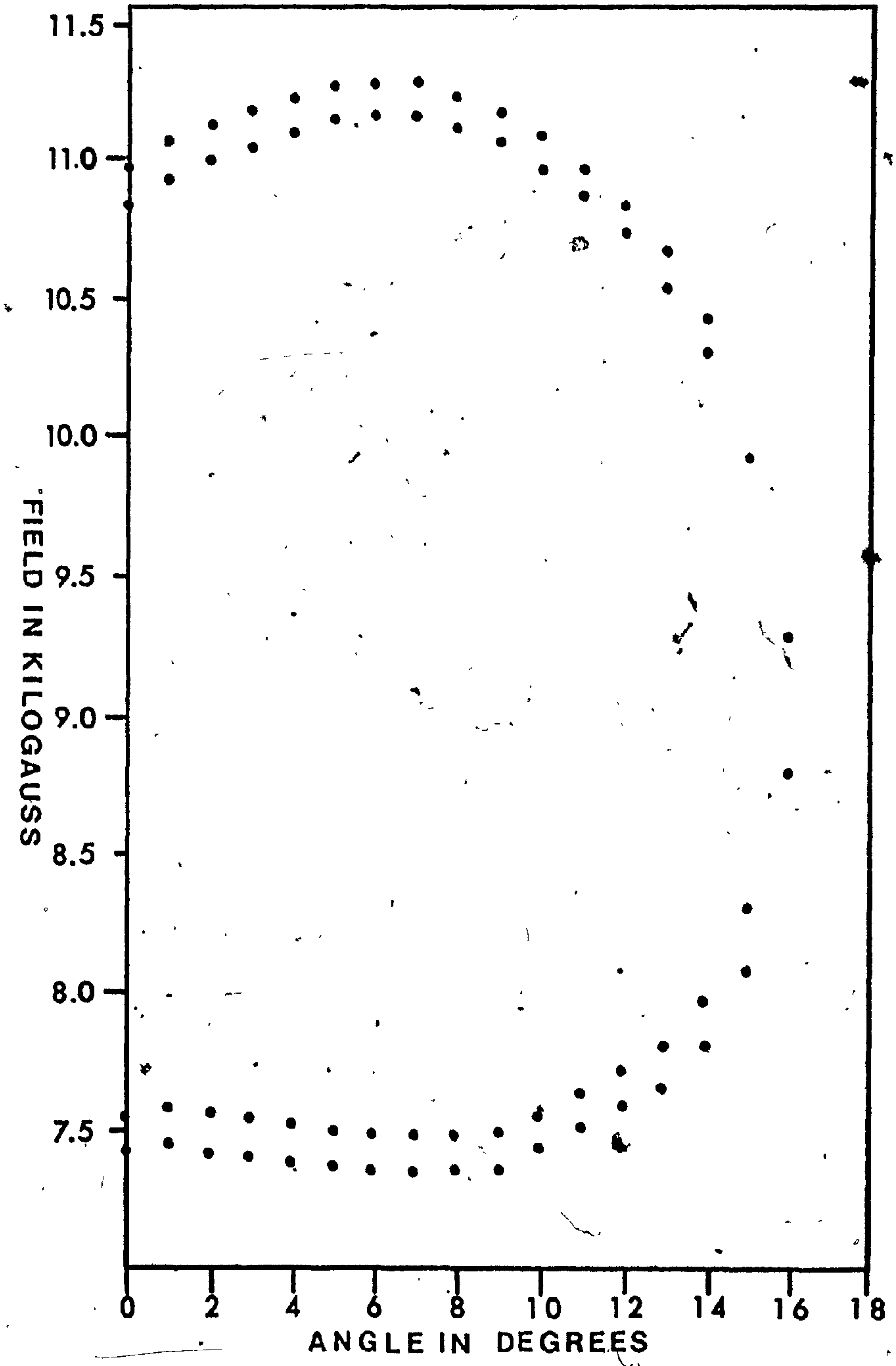

Fig. 5.6. Angular variation of the 5/2 ↔ 1/2 transition for sites I and II in the ZX plane.

transitions. In fact they only gave good results for four out of the eight lines observed. It should be noted that Brock et. al.[3] only reported these four transitions along the Z-axis.

Using the following identification of transitions and magnetic field values a new set of parameters are calculated.

Transition	Magnetic Field (Gauss)
5/2 ↔ -1/2	10964
3/2 ↔ 1/2	9813
1/2 ↔ -1/2	3352

This implies that a 5/2 ↔ 3/2 line should lie at a higher magnetic field value. This line is calculated to be 15589 Gauss, above the limit of the magnetic field. Evidence of a higher field line can be seen at 2.5 degrees from the Z-axis. Table 5.1 gives the diagonal parameters for sites I and II and Table 5.2 gives the transitions, the experimental magnetic field value and the calculated magnetic field value along the Z-axis.

Table 5.1 Diagonal parameters calculated for sites I and II along the Z-axis. Here $b_2^m = 3B_2^m$ and $b_4^m = 60B_4^m$.

Parameter	Site I	Site II
g_{zz}	2.004	2.004
b_2^0	-8.659	-8.531
b_4^0	0.162	0.160

Table 5.2 Experimental and calculated magnetic field values for sites I and II along the Z-axis.

SITE I

Transition	Experimental Mag. Field (Gauss)	Calculated Mag. Field (Gauss)	Difference (Gauss)
5/2 ↔ 1/2	10964	10964	0
3/2 ↔ 1/2	9813	9813	0
5/2 ↔ 3/2	8705	8763	-58
5/2 ↔ 1/2	7570	7612	-42
3/2 ↔ -1/2	4923	4906	17
1/2 ↔ -1/2	3352	3352	0
3/2 ↔ 1/2	3132	3109	23
3/2 ↔ -1/2	1565	1554	11

SITE II

Transition	Experimental Mag. Field (Gauss)	Calculated Mag. Field (Gauss)	Difference (Gauss)
5/2 ↔ 1/2	10827	10827	0
3/2 ↔ 1/2	9718	9718	0
5/2 ↔ 3/2	8524	8584	-60
5/2 ↔ 1/2	7433	7475	-42
3/2 ↔ -1/2	4880	4859	21
1/2 ↔ -1/2	3352	3352	0
3/2 ↔ 1/2	3040	3014	26
3/2 ↔ -1/2	1517	1507	10

Considering the fact that the off-diagonal elements of the spin Hamiltonian have been neglected, the agreement between experimental and calculated magnetic field values is found to be excellent noting the small difference in Table 5.2.

In order to verify that the parameters indeed characterize the spectrum of Fe^{3+} in GASH a rigorous least-squares procedure is used to fit all the observed lines in the ZX plane at angles of 0, 10, 20, 30, 40, 50, 60, 70, 80, 90 degrees from the Z-axis. This means taking simultaneously into consideration 44 magnetic field values. Thus the values of the seven parameters g_{zz}, g_{xx}, g_{zx}, B_2^0, B_4^0, B_4^3, B_4^{-3} are obtained from a rather large number of lines (about 6 times as many lines as the number of parameters). The initial values for the least-squares fitting program are those calculated using the diagonal elements only and putting $g_{zz} = g_{xx}$. The initial values for g_{zx}, B_4^3 and B_4^{-3} are taken to be zero.

Table 5.3 gives the parameters for Fe^{3+} in GASH at room temperature for sites I and II. As well the $\text{SSMD} = (\sum_{jk} |\Delta E_{jk}| - h\nu)^2$ is given. [Here ν is the microwave frequency (9.4038 gHz), h is Planck's constant, $\Delta E_{jk} = E_j - E_k$; E_j and E_k are the energies of the levels between which the microwave energy is being absorbed].

It is noted that the value of b_2^0 reported here is about twice in magnitude to that reported in Ref. (3). This is not surprising since the parameters quoted in Ref. (3) are calculated using only four lines at X-band frequencies for the magnetic field orientation along the Z-axis.

Table 5.3 Values of parameters characterizing the EPR data for Fe^{3+} in GASH at 9.4038 gHz at 295 K. The units of the non-Zeeman parameters is gHz. Here $b_2^m = 3B_2^m$ and $b_4^m = 60B_4^m$. The values enclosed in brackets are those determined by Brock et. al.

	SITE I		SITE II	
g_{zz}	2.001 ±.003	(2.003)	2.002 ±.003	(2.003)
g_{xx}	2.004 ±.003	-	2.002 ±.003	-
g_{zx}	0.001 ±.003	-	0.001 ±.003	-
b_2^0	-8.622 ±.008	(-5.552)	-8.499 ±.008	(-5.280)
b_4^0	0.181 ±.008	(-0.028)	0.181 ±.008	(-0.027)
b_4^3	0.531 ±.008	(0.052)	0.184 ±.008	(0.049)
b_4^{-3}	-2.712 ±.008	-	-2.945 ±.008	-
SSMD	0.069	-	0.053	

Using the parameters for site I of Table 5.3, the variations of eigenvalues as functions of static magnetic field orientation in the ZX plane at angles of 0 and 90 degrees from the Z-axis are shown in Figs. 5.7 and 5.8 respectively. The zero field splittings for room temperature are as follows. Site I: E(±1/2) = 23.36 ± .10 gHz, E(±3/2) = 5.21 ± .10 gHz,

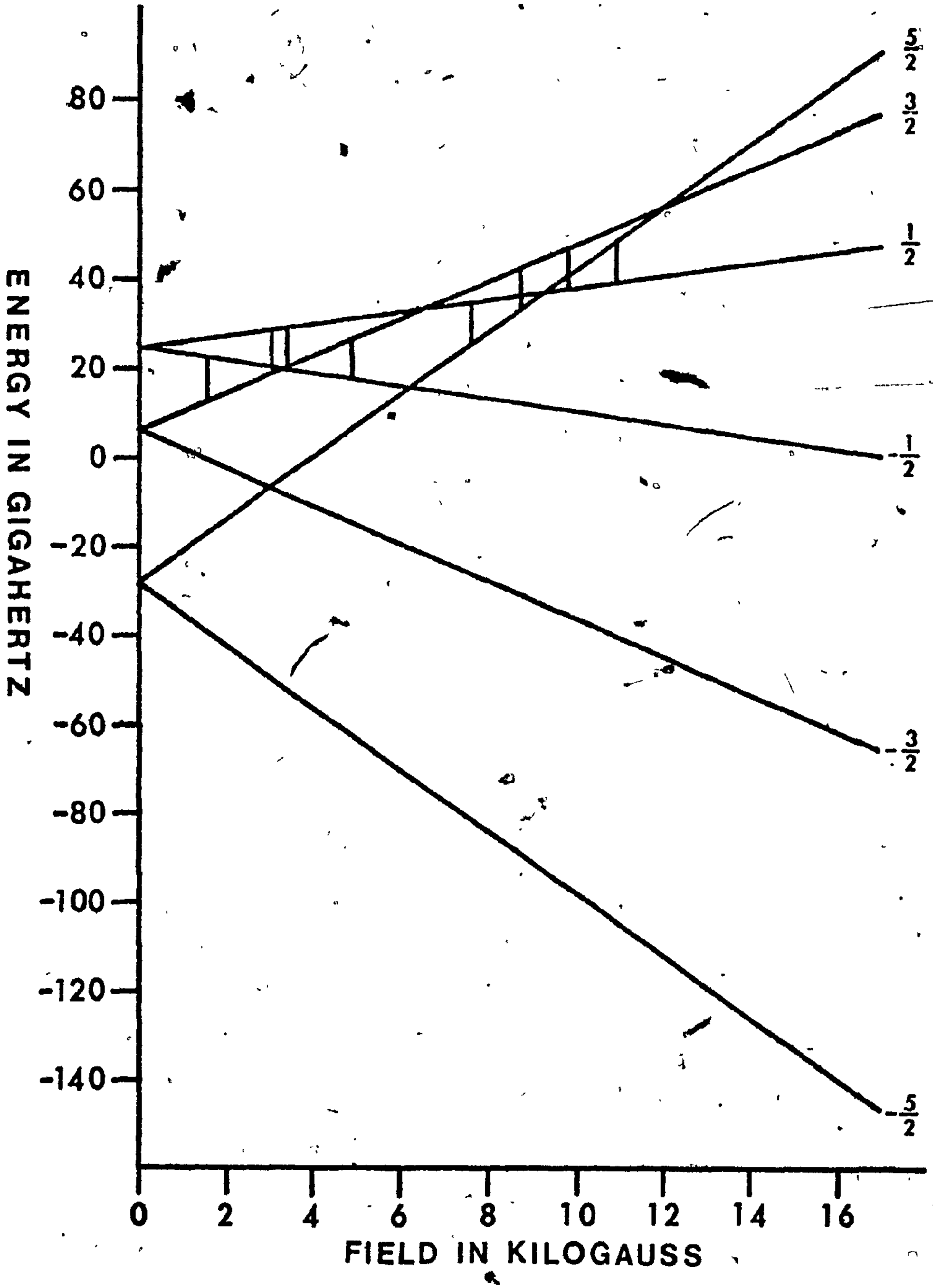

Fig. 5.7. The variations of eigenvalues as functions of static magnetic field directed along the Z-axis.

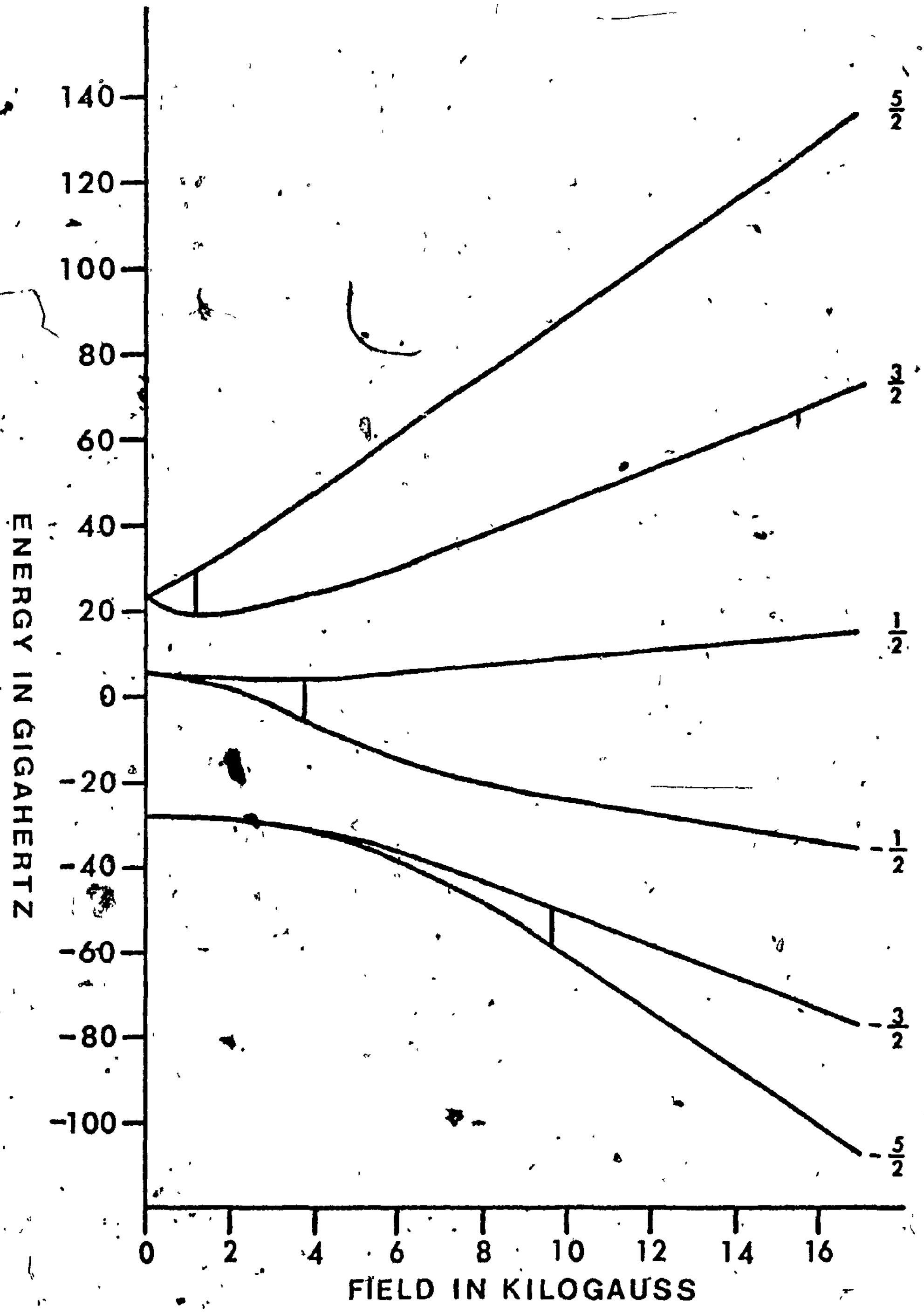

Fig. 5.8. The variation of eigenvalues as functions of static magnetic field directed along the X-axis.

E(±5/2) = -28.56 ± .10 gHz; Site II: E(±1/2) = 23.03 ± .10 gHz, E(±3/2) = 5.12 ± .10 gHz, E(±5/2) = -28.15 ± .10 gHz (the numbers in parenthesis represent magnetic quantum numbers).

Tables 5.4 and 5.5 give the magnetic field values of the lines measured at each angle and the SMD = $(|\Delta E_{jk}| - h\nu)^2$ for site I and site II respectively.

Table 5.4 The magnetic field of each line at each orientation of the static magnetic field and the SMD in the ZX plane for site I at room temperature. The angle is measured from the Z-axis.

Angle (Degrees)	Magnetic Field (Gauss)	SMD (gHz^2)
0	1565	$.343 \times 10^{-3}$
0	3132	$.705 \times 10^{-3}$
0	3352	$.436 \times 10^{-3}$
0	4923	$.727 \times 10^{-4}$
0	7570	$.785 \times 10^{-2}$
0	8705	$.861 \times 10^{-3}$
0	9813	$.455 \times 10^{-2}$
0	10964	$.109 \times 10^{-1}$
10	1556	$.210 \times 10^{-4}$
10	2981	$.181 \times 10^{-3}$
10	3899	$.173 \times 10^{-2}$
10	5128	$.103 \times 10^{-3}$

Table 5.4 Cont'd

Angle (Degrees)	Magnetic Field (Gauss)	SMD (gHz^2)
10	7530	.270 x 10^{-2}
10	11054	.584 x 10^{-3}
20	1568	.200 x 10^{-3}
20	2413	.918 x 10^{-4}
20	5023	.593 x 10^{-3}
20	5274	.300 x 10^{-3}
20	7899	.144 x 10^{-4}
30	1306	.189 x 10^{-3}
30	1651	.891 x 10^{-3}
30	1982	.38[illegible] 10^{-4}
30	5787	.280 x 10^{-2}
30	7819	.127 x 10^{-1}
40	1502	.185 x 10^{-4}
40	1682	.134 x 10^{-3}
40	1927	.164 x 10^{-2}
40	3390	.111 x 10^{-3}
40	5177	.562 x 10^{-4}
50	1477	.368 x 10^{-4}
50	1847	.166 x 10^{-3}
50	3332	.727 x 10^{-3}
50	6218	.637 x 10^{-3}
60	1341	.303 x 10^{-4}
60	2464	.539 x 10^{-3}

Table 5.4 Cont'd

Angle (Degrees)	Magnetic Field (Gauss)	SMD (gHz^2)
60	4220	$.101 \times 10^{-3}$
60	7115	$.775 \times 10^{-2}$
70	1256	$.241 \times 10^{-3}$
70	3199	$.208 \times 10^{-3}$
80	1209	$.543 \times 10^{-3}$
80	3685	$.166 \times 10^{-2}$
90	1194	$.672 \times 10^{-3}$
90	3846	$.359 \times 10^{-2}$
90	9729	$.728 \times 10^{-3}$

Table 5.5 The magnetic field of each line at each orientation of the static magnetic field and the SMD in the ZX plane for site II at room temperature. The angle is measured from the Z-axis.

Angle (Degrees)	Magnetic Field (Gauss)	SMD (gHz^2)
0	1517	$.276 \times 10^{-4}$
0	3040	$.205 \times 10^{-3}$
0	3352	$.401 \times 10^{-3}$
0	4880	$.191 \times 10^{-3}$
0	7433	$.113 \times 10^{-1}$
0	8524	$.507 \times 10^{-3}$
0	9718	$.699 \times 10^{-2}$

Table 5.5 Cont'd

Angle (Degrees)	Magnetic Field (Gauss)	SMD (gHz^2)
0	10827	$.777 \times 10^{-2}$
10	1512	$.243 \times 10^{-4}$
10	2981	$.658 \times 10^{-3}$
10	3747	$.886 \times 10^{-3}$
10	5088	$.414 \times 10^{-4}$
10	7380	$.555 \times 10^{-3}$
10	10929	$.147 \times 10^{-2}$
20	1522	$.153 \times 10^{-3}$
20	2413	$.366 \times 10^{-3}$
20	4985	$.112 \times 10^{-5}$
20	5176	$.242 \times 10^{-3}$
20	7805	$.308 \times 10^{-2}$
30	1306	$.173 \times 10^{-3}$
30	1594	$.423 \times 10^{-4}$
30	1982	$.733 \times 10^{-4}$
30	5667	$.399 \times 10^{-3}$
30	7777	$.506 \times 10^{-2}$
40	1502	$.113 \times 10^{-5}$
40	1682	$.540 \times 10^{-4}$
40	1844	$.755 \times 10^{-3}$
40	3390	$.660 \times 10^{-4}$
40	5121	$.155 \times 10^{-3}$

Table 5.5 Cont'd

Angle (Degrees)	Magnetic Field (Gauss)	SMD (gHz^2)
50	1477	$.246 \times 10^{-3}$
50	1847	$.396 \times 10^{-5}$
50	3256	$.213 \times 10^{-3}$
50	6154	$.323 \times 10^{-3}$
60	1341	$.330 \times 10^{-3}$
60	2464	$.971 \times 10^{-4}$
60	4126	$.165 \times 10^{-3}$
60	7069	$.888 \times 10^{-2}$
70	1256	$.907 \times 10^{-4}$
70	3199	$.131 \times 10^{-4}$
80	1209	$.714 \times 10^{-5}$
80	3685	$.212 \times 10^{-3}$
90	1194	$.364 \times 10^{-6}$
90	3846	$.833 \times 10^{-4}$
90	9641	$.189 \times 10^{-3}$

5.1.2. Spectrum at 79.0 K

The spectra of Fe^{3+} in GASH was measured in the ZX plane at 79.0 K and is found to exhibit the same symmetry as that observed at room temperature. The data is first analyzed using the Z-axis resonant magnetic field values using Eq. 17

in order to obtain the initial parameters to be used in the least-squares fitting program. Table 5.6 is a summary these parameters.

Table 5.6 Diagonal parameters calculated for sites I and II along the Z-axis. Here $b_2^m = 3B_2^m$ and $b_4^m = 60B_4^m$.

Parameter	Site I	Site II
g_{zz}	2.004	2.004
b_2^0	-8.965	-8.823
b_4^0	0.156	0.148

The least-squares fitting procedure is now used to fit all the lines observed in the ZX plane at angles of 0, 10, 20, 30, 40, 50, 60, 70, 80, 90 degrees from the Z-axis. This means taking simultaneously into account 42 lines. Table 5.7 gives the parameters and the SSMD for Fe^{3+} in GASH at 78.99 K for sites I and II.

Table 5.7 Values of parameters characterizing the EPR data for Fe^{3+} in GASH at 9.4151 gHz at 78.99 K. The units of the non-Zeeman parameters are gHz. Here $b_2^m = 3B_2^m$ and $b_4^m = 60B_4^m$. The values enclosed in brackets are those determined by Brock et. al.

	SITE I		SITE II	
g_{zz}	1.995 ±.003	(2.003)	1.997 ±.003	(2.003)
g_{xx}	2.004 ±.003	-	2.005 ±.003	-
g_{zx}	0.006 ±.003	-	0.005 ±.003	-
b_2^0	-8.888 ±.008	(-5.852)	-8.765 ±.008	(-5.671)
b_4^0	0.173 ±.008	(-0.035)	0.173 ±.008	(-0.033)
b_4^3	2.963 ±.008	(0.139)	2.763 ±.008	(0.127)
b_4^{-3}	-1.226 ±.008	-	-3.397 ±.008	-

The parameters for for sites I and II of Table 5.7 yield the following zero field splittings. Site I: E(±1/2) = 24.05 ± .10 gHz, E(±3/2) = 5.41 ± .10 gHz, E(±5/2) = -29.46 ± .10 gHz; Site II: E(±1/2) = 23.71 ± .10 gHz, E(±3/2) = 5.32 ± .10 gHz, E(±5/2) = -29.03 ± .10 gHz.

Tables 5.8 and 5.9 give the magnetic field lines measured at each angle and the SMD for sites I and II respectively.

Table 5.8 The magnetic field of each line at each orientation of the static magnetic field and the SMD in the ZX plane for site I at 78.99 K. The angle is measured from the Z-axis.

Angle (Degrees)	Magnetic Field (Gauss)	SMD (gHz^2)
0	1646	$.253 \times 10^{-1}$
0	3347	$.272 \times 10^{-1}$
0	3357	$.198 \times 10^{-2}$
0	5056	$.199 \times 10^{-1}$
0	7880	$.758 \times 10^{-2}$
0	9157	$.124 \times 10^{-1}$
0	10028	$.981 \times 10^{-2}$
0	11296	$.532 \times 10^{-2}$
10	1650	$.832 \times 10^{-2}$
10	2994	$.190 \times 10^{-2}$
10	4174	$.930 \times 10^{-3}$
10	5256	$.220 \times 10^{-2}$
10	7829	$.456 \times 10^{-2}$
10	11403	$.678 \times 10^{-1}$
20	1667	$.211 \times 10^{-2}$
20	2388	$.515 \times 10^{-2}$
20	5174	$.782 \times 10^{-2}$
20	5486	$.314 \times 10^{-1}$
20	8043	$.107 \times 10^{-1}$

Table 5.8 Cont'd

Angle (Degrees)	Magnetic Field (Gauss)	SMD (gHz^2)
30	1290	$.193 \times 10^{-1}$
30	1749	$.433 \times 10^{-3}$
30	1978	$.536 \times 10^{-3}$
30	6108	$.241 \times 10^{-1}$
30	7911	$.218 \times 10^{-1}$
40	1503	$.112 \times 10^{-3}$
40	1650	$.145 \times 10^{-1}$
40	2142	$.195 \times 10^{-1}$
40	3322	$.326 \times 10^{-1}$
40	5354	$.905 \times 10^{-1}$
50	1486	$.746 \times 10^{-2}$
50	1814	$.123 \times 10^{-1}$
50	6272	$.561 \times 10^{-1}$
60	1322	$.827 \times 10^{-2}$
60	4402	$.321 \times 10^{-3}$
60	7092	$.839 \times 10^{-2}$
70	1240	$.539 \times 10^{-2}$
70	3158	$.122 \times 10^{-1}$
80	1191	$.788 \times 10^{-2}$
80	3683	$.482 \times 10^{-2}$
90	1188	$.791 \times 10^{-4}$
90	3935	$.146 \times 10^{-1}$
90	9962	$.827 \times 10^{-2}$

Table 5.9 The magnetic field of each line at each orientation of the static magnetic field and the SMD in the ZX plane for site II at 78.99 K. The angle is measured from the Z-axis.

Angle (Degrees)	Magnetic Field (Gauss)	SMD (gHz^2)
0	1580	$.231 \times 10^{-1}$
0	3274	$.294 \times 10^{-1}$
0	3357	$.338 \times 10^{-2}$
0	5008	$.142 \times 10^{-1}$
0	7732	$.986 \times 10^{-2}$
0	8962	$.102 \times 10^{-1}$
0	9913	$.134 \times 10^{-1}$
0	11143	$.566 \times 10^{-2}$
10	1617	$.980 \times 10^{-2}$
10	2994	$.127 \times 10^{-2}$
10	4043	$.936 \times 10^{-3}$
10	5207	$.779 \times 10^{-3}$
10	7682	$.608 \times 10^{-2}$
10	11288	$.603 \times 10^{-1}$
20	1602	$.138 \times 10^{-2}$
20	2388	$.580 \times 10^{-2}$
20	5125	$.691 \times 10^{-2}$
20	5387	$.354 \times 10^{-1}$
20	7944	$.158 \times 10^{-1}$

Table 5.9 Cont'd

Angle (Degrees)	Magnetic Field (Gauss)	SMD (gHz^2)
30	1290	$.226 \times 10^{-1}$
30	1699	$.865 \times 10^{-3}$
30	1978	$.404 \times 10^{-3}$
30	5977	$.267 \times 10^{-1}$
30	7846	$.219 \times 10^{-1}$
40	1503	$.430 \times 10^{-6}$
40	1650	$.152 \times 10^{-1}$
40	2044	$.213 \times 10^{-1}$
40	3322	$.315 \times 10^{-1}$
40	5289	$.841 \times 10^{-1}$
50	1486	$.702 \times 10^{-2}$
50	1814	$.148 \times 10^{-1}$
50	6207	$.616 \times 10^{-1}$
60	1322	$.876 \times 10^{-2}$
60	4337	$.386 \times 10^{-3}$
60	7026	$.750 \times 10^{-2}$
70	1240	$.583 \times 10^{-2}$
70	3158	$.129 \times 10^{-1}$
80	1191	$.848 \times 10^{-2}$
80	3683	$.451 \times 10^{-2}$
90	1188	$.160 \times 10^{-3}$
90	3907	$.993 \times 10^{-2}$
90	9866	$.157 \times 10^{-1}$

5.1.3. Spectrum at 1.6 K

The spectra of Fe^{3+} in GASH was measured in the ZX plane at 1.6 K and is found to exhibit the same symmetry as that observed at room temperature. The data is again analyzed using the Z-axis resonant magnetic field values to obtain the initial parameters for the least-squares fitting program. Table 5.10 is a summary of the diagonal parameters for both sites I and II

Table 5.10 Diagonal parameters calculated for sites I and II along the Z-axis. Here $b_2^m = 3B_2^m$ and $b_4^m = 60B_4^m$.

Parameter	Site I	Site II
g_{zz}	2.003	2.003
b_2^0	-8.991	-8.858
b_4^0	0.178	0.184

All the lines observed in the ZX plane at angles of 0, 30, 45, 60, 90 degrees from the Z-axis (23 lines) are simultaneously considered for fitting, the resulting parameters are listed in Table 5.11.

Table 5.11 Values of parameters characterizing the EPR data for Fe^{3+} in GASH at 9.2117 gHz at 1.61 K. The units of the non-Zeeman parameters are gHz. Here $b_2^m = 3B_2^m$ and $b_4^m = 60\ B_4^m$.

	SITE I	SITE II
g_{zz}	1.994 ±.003	1.996 ±.003
g_{xx}	1.992 ±.003	1.997 ±.003
g_{zx}	0.009 ±.003	0.008 ±.003
b_2^0	-8.931 ±.008	-8.808 ±.008
b_4^0	0.193 ±.008	0.199 ±.008
b_4^3	2.998 ±.008	3.271 ±.008
b_4^{-3}	-3.441 ±.008	-2.204 ±.008

The parameters for sites I and II give the following zero field splittings. Site I: E(±1/2) = 24.21 ± .10 gHz, E(±3/2) = 5.38 ± .10 gHz, E(±5/2) = -29.58 ± .10 gHz; Site II: E(±1/2) = 23.89 ± .10 gHz, E(±3/2) = 5.27 ± .10 gHz, E(±5/2) = -29.17 ± .10 gHz.

Tables 5.12 and 5.13 give the magnetic field values of the lines measured at each angle at 1.61 K and the SMD for sites I and II respectively.

Table 5.12 The magnetic field of each line at each orientation of the static magnetic field and the SMD in the ZX plane for site I at 1.61 K. The angle is measured from the Z-axis.

Angle (Degrees)	Magnetic Field (Gauss)	SMD (gHz^2)
0	1736	$.372 \times 10^{-2}$
0	3467	$.262 \times 10^{-2}$
0	3285	$.299 \times 10^{-2}$
0	5023	$.236 \times 10^{-2}$
0	7978	$.408 \times 10^{-4}$
0	9245	$.432 \times 10^{-2}$
0	10015	$.542 \times 10^{-2}$
0	11293	$.157 \times 10^{-2}$
30	1291	$.551 \times 10^{-2}$
30	1862	$.110 \times 10^{-1}$
30	1947	$.685 \times 10^{-2}$
30	6253	$.118 \times 10^{-2}$
30	7841	$.617 \times 10^{-2}$
45	1557	$.262 \times 10^{-1}$
45	1609	$.155 \times 10^{-2}$
45	5742	$.402 \times 10^{-2}$
60	1323	$.267 \times 10^{-2}$
60	2362	$.227 \times 10^{-3}$
60	4479	$.124 \times 10^{-2}$
60	7057	$.168 \times 10^{-1}$

Table 5.12 Cont'd

Angle (Degrees)	Magnetic Field (Gauss)	SMD (gHz^2)
90	1188	$.269 \times 10^{-1}$
90	3889	$.167 \times 10^{-2}$
90	9888	$.396 \times 10^{-2}$

Table 5.13 The magnetic field of each line at each orientation of the static magnetic field and the SMD in the ZX plane for site II at 1.61 K. The angle is measured from the Z-axis

Angle (Degrees)	Magnetic Field (Gauss)	SMD (gHz^2)
0	1688	$.536 \times 10^{-3}$
0	3376	$.691 \times 10^{-3}$
0	3285	$.169 \times 10^{-2}$
0	4976	$.262 \times 10^{-2}$
0	7836	$.764 \times 10^{-4}$
0	9054	$.664 \times 10^{-2}$
0	9930	$.427 \times 10^{-2}$
0	11152	$.394 \times 10^{-2}$
30	1291	$.639 \times 10^{-2}$
30	1817	$.156 \times 10^{-1}$
30	1947	$.813 \times 10^{-2}$
30	6122	$.606 \times 10^{-2}$
30	7735	$.205 \times 10^{-2}$

Table 5.13 Cont'd

Angle (Degrees)	Magnetic Field (Gauss)	SMD (gHz^2)
45	1557	$.285 \times 10^{-1}$
45	1609	$.143 \times 10^{-2}$
45	5676	$.451 \times 10^{-2}$
60	1323	$.272 \times 10^{-2}$
60	2362	$.365 \times 10^{-2}$
60	4388	$.670 \times 10^{-3}$
60	6988	$.611 \times 10^{-2}$
90	1162	$.100 \times 10^{-3}$
90	3862	$.104 \times 10^{-2}$
90	9708	$.445 \times 10^{-3}$

CHAPTER VI

EXPERIMENTAL DETAILS AND ANALYSIS OF THE DATA FOR Fe^{3+} IN $(NH_4)_2InCl_5 \cdot H_2O$

The crystals were grown from an aqueous solution of calculated amounts of ammonium chloride, indium chloride and ferric chloride so as to have a starting ratio of one Fe^{3+} ion for every ten In^{3+} ion.[3] The solution was made slightly acidic with hydrochloric acid to prevent hydrolysis of the ferric ions. The solution was allowed to slowly evaporate from a partially covered beaker at room temperature and the crystals were allowed to grow to sizes compatible with X-band cavity dimensions.

The crystal growing habits are shown in in Fig. 6.1. For measurements in the ac-plane crystal growth habit (a) of the crystal is used for mounting at $\lambda_g/4$ from the top of the cavity with the a-face against the smallest cavity wall and the b-axis pointing upwards. For measurements in the bc-plane the crystal is placed on the bottom of the cavity with the a-axis pointing upwards. For the ab-plane growth habit (b) of the crystal is used and mounted at $\lambda_g/4$ from the top of the cavity on an r-face with the c-axis pointing upwards.

6.1. Spectrum at 295 K

The spectrum was investigated in the ab and bc-planes

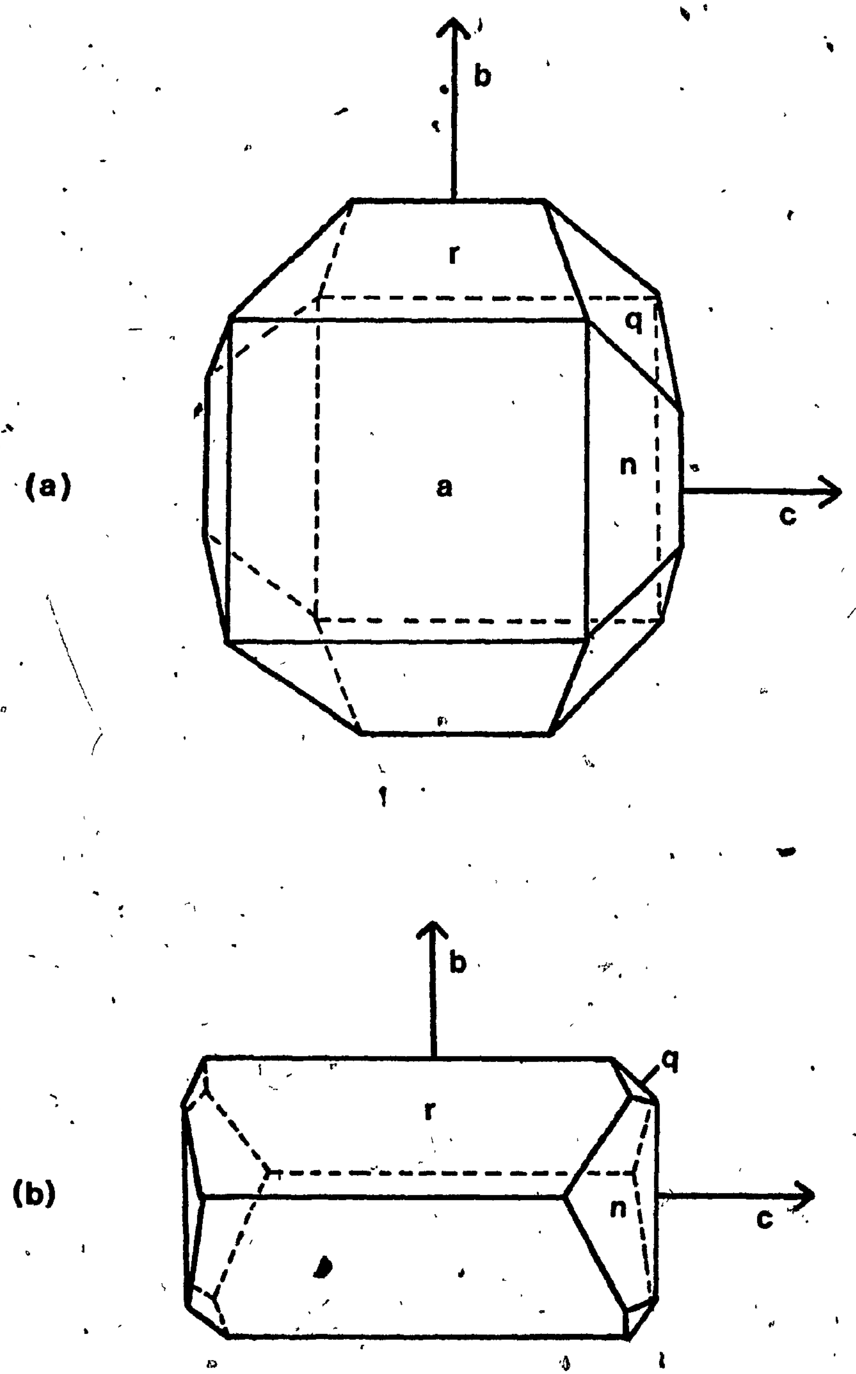

Fig. 6.1. Crystal growing habits of di-ammonium indium pentachloride monohydrate

for both sites I and II and the angular variations are shown in Figs. 6.2 and 6.3. From the crystalline structure, the spectra for the two sites should overlap completely, and are expected to be of equal intensity. Indeed they do overlap (except, perhaps, for small splittings of the lines at some intermediate angles). Along the crystalline b-axis (X-axis of the g-tensor) all the lines overlap completely as shown in Fig. 6.4, thus indicating that the parameters for the two sites are identical. Figures 6.5 and 6.6 show the unsplit spectrum along the a and c crystalline axes respectively.

Figures 6.7 and 6.8 show the spectrum along the Z and Y-axes of site I respectively. The lines are labelled I and II refering to sites I and II respectively. These axes are contained in the angular variation in the ac-plane of the crystal as shown in Fig. 6.9 where the lines corresponding to site I have been connected by solid lines and those corresponding to site II are left unconnected. The two Z-axes, one for each site, lie in the ac-plane at angles of ± (40.00 ± 0.25°) from the a-axis. The X-ray data[6] indicates the $H_2O\text{-}Fe^{3+}\text{-}Cl^-$ axis forms an angle of 38°40' with the a-axis which is an axis of near tetragonal symmetry. It is noted that the spectra for each site overlap completely along the a and c-axes.

In the least-squares fitting procedure used for the analysis, the data along the X, Y, Z and 20, 30, 40, 50, 60, and 70 degrees from the Z-axis in the ZY-plane are simultaneously

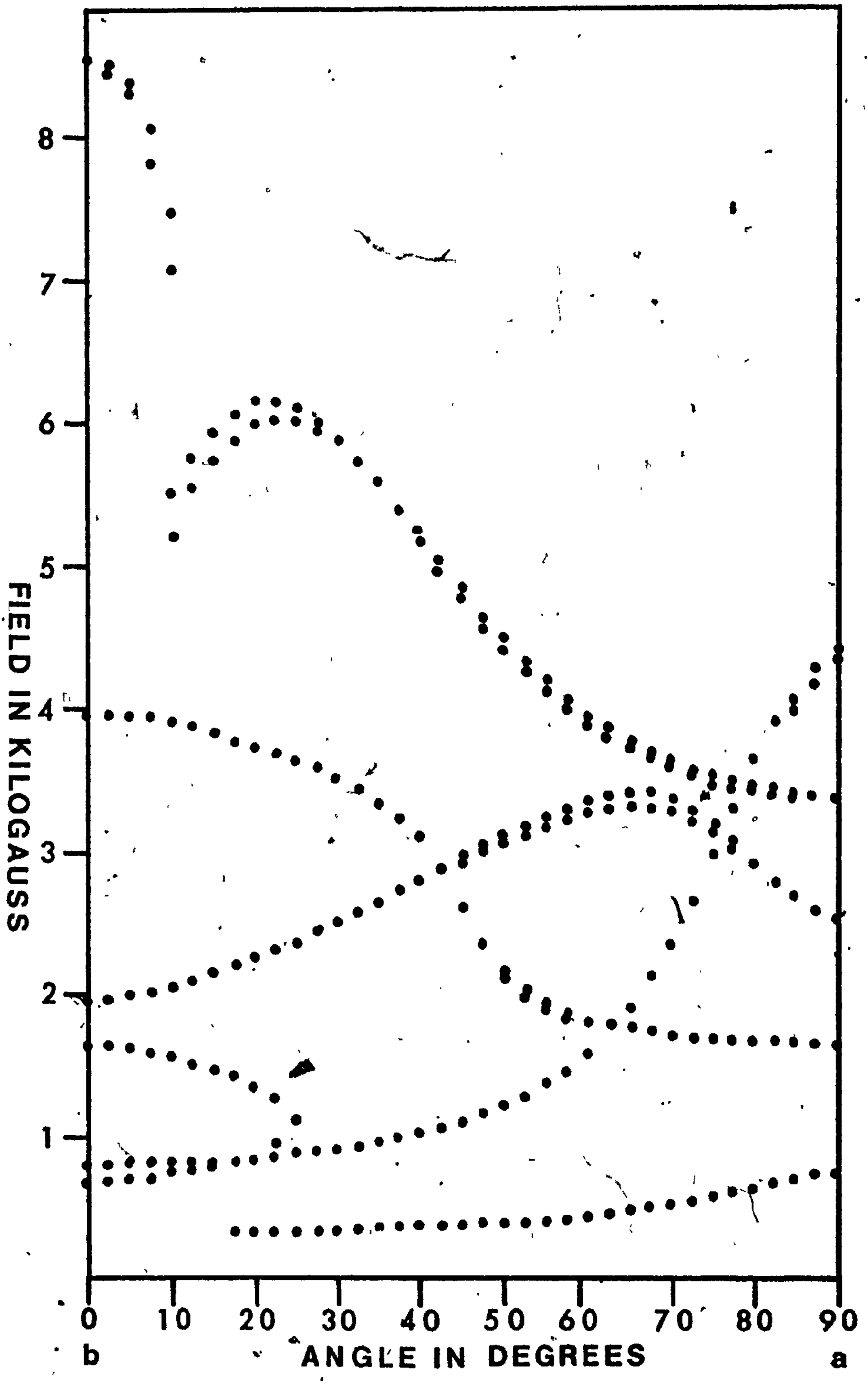

Fig. 6.2. - The spectral angular variation for the static magnetic field in the ab plane.

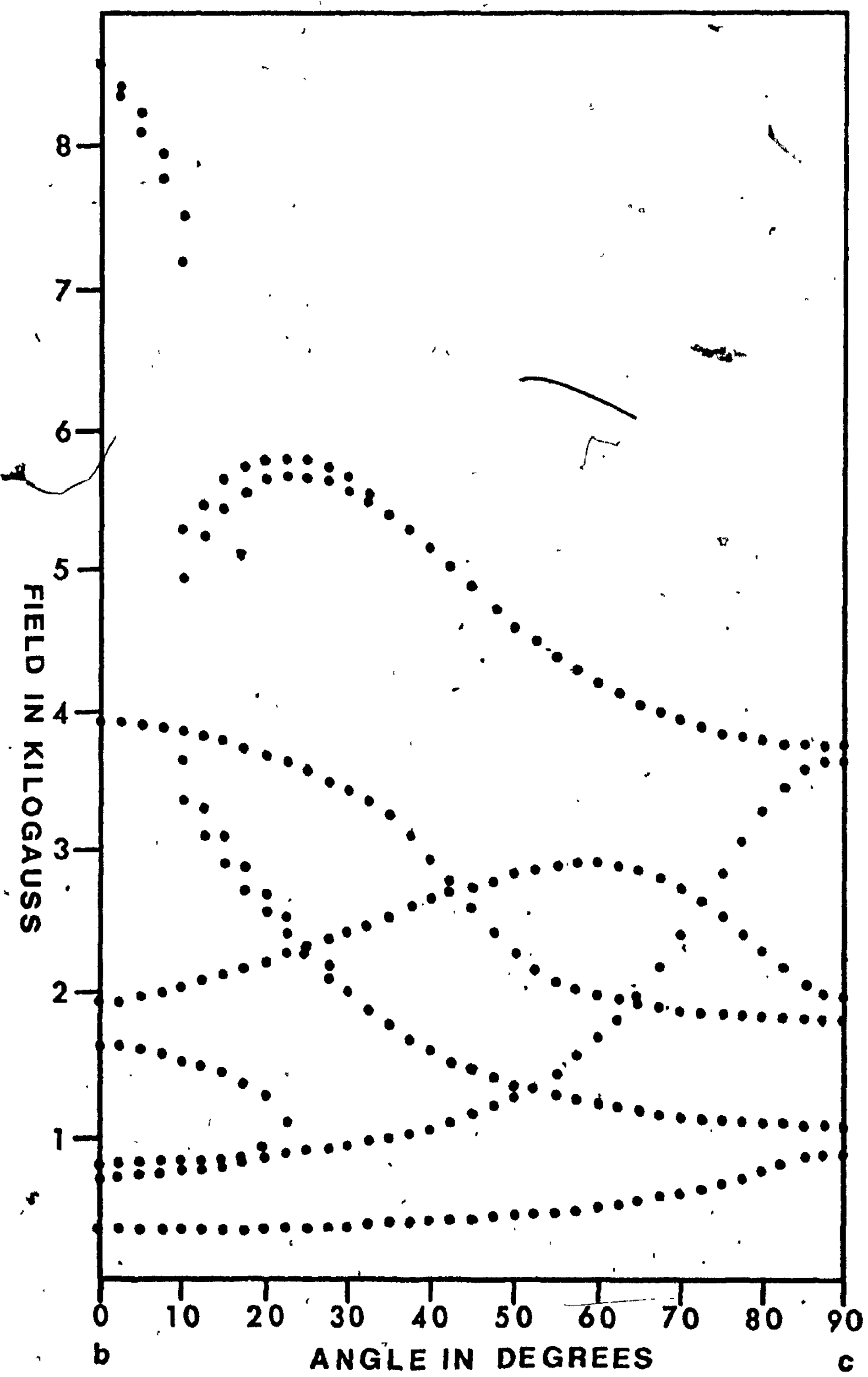

Fig. 6.3. The spectral angular variation for the static magnetic field in the bc plane.

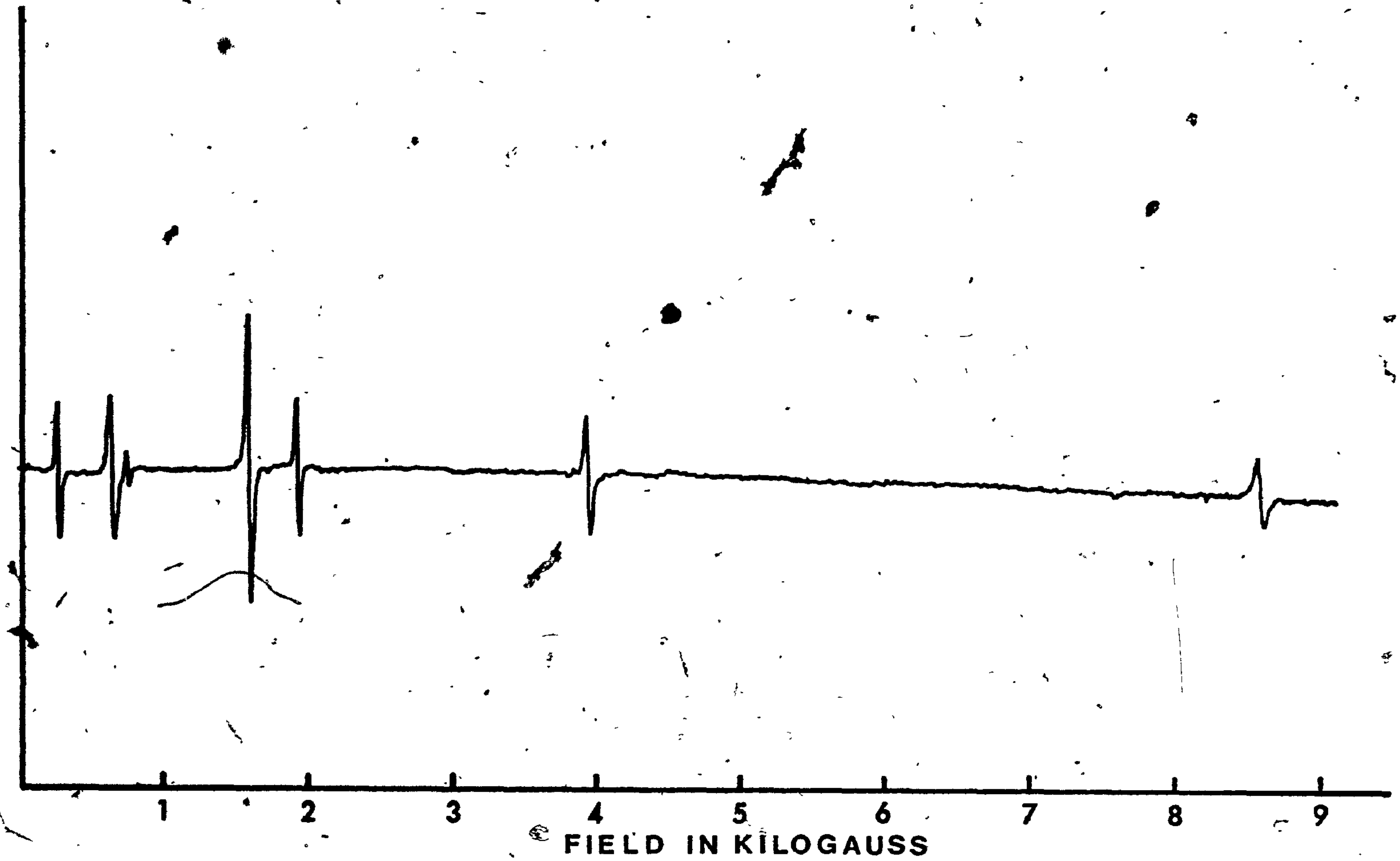

Fig 6.4. EPR absorption spectrum with the static magnetic field directed along the b-axis.

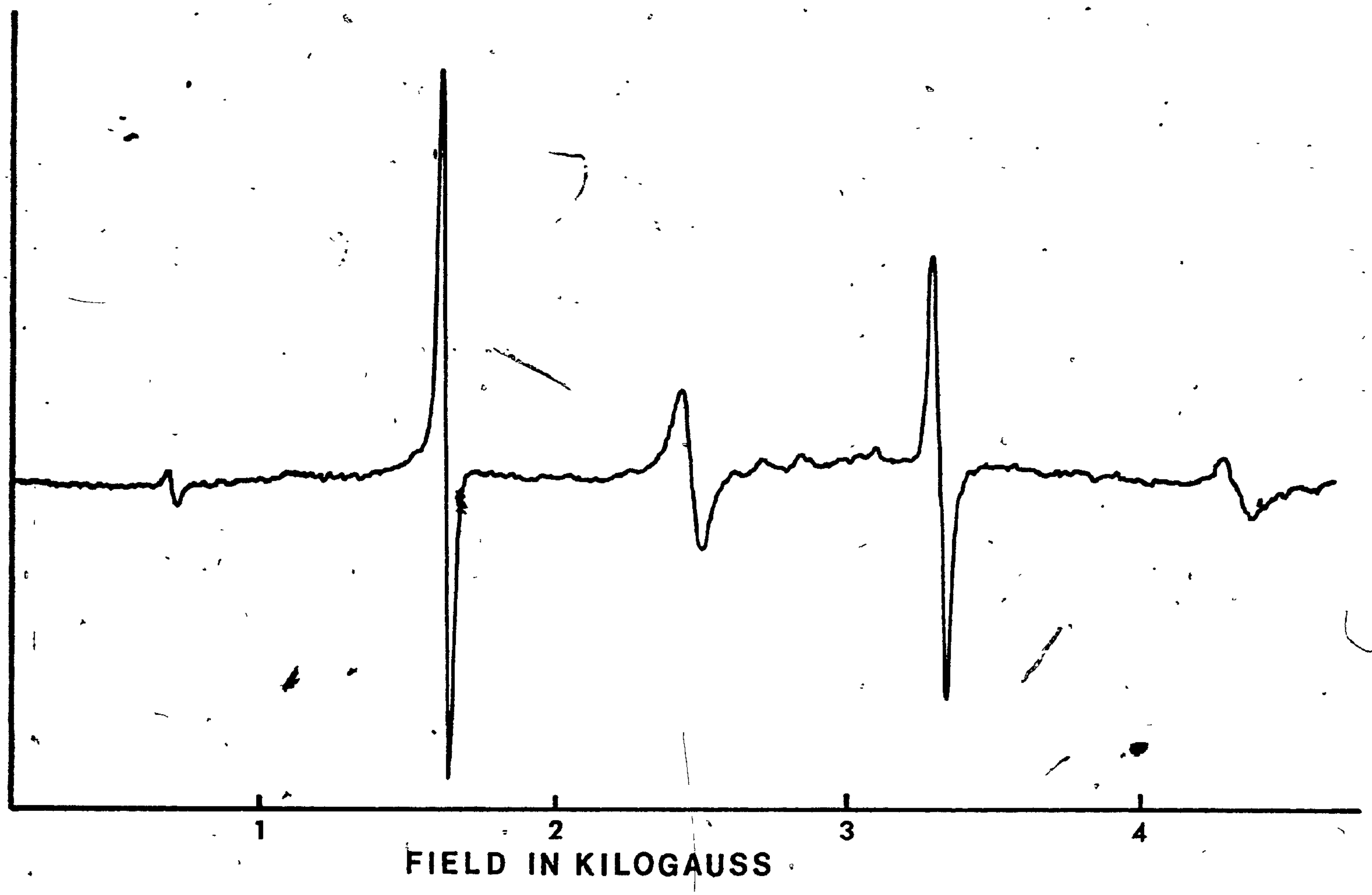

Fig. 6.5. EPR absorption spectrum with the static magnetic field directed along the a-axis.

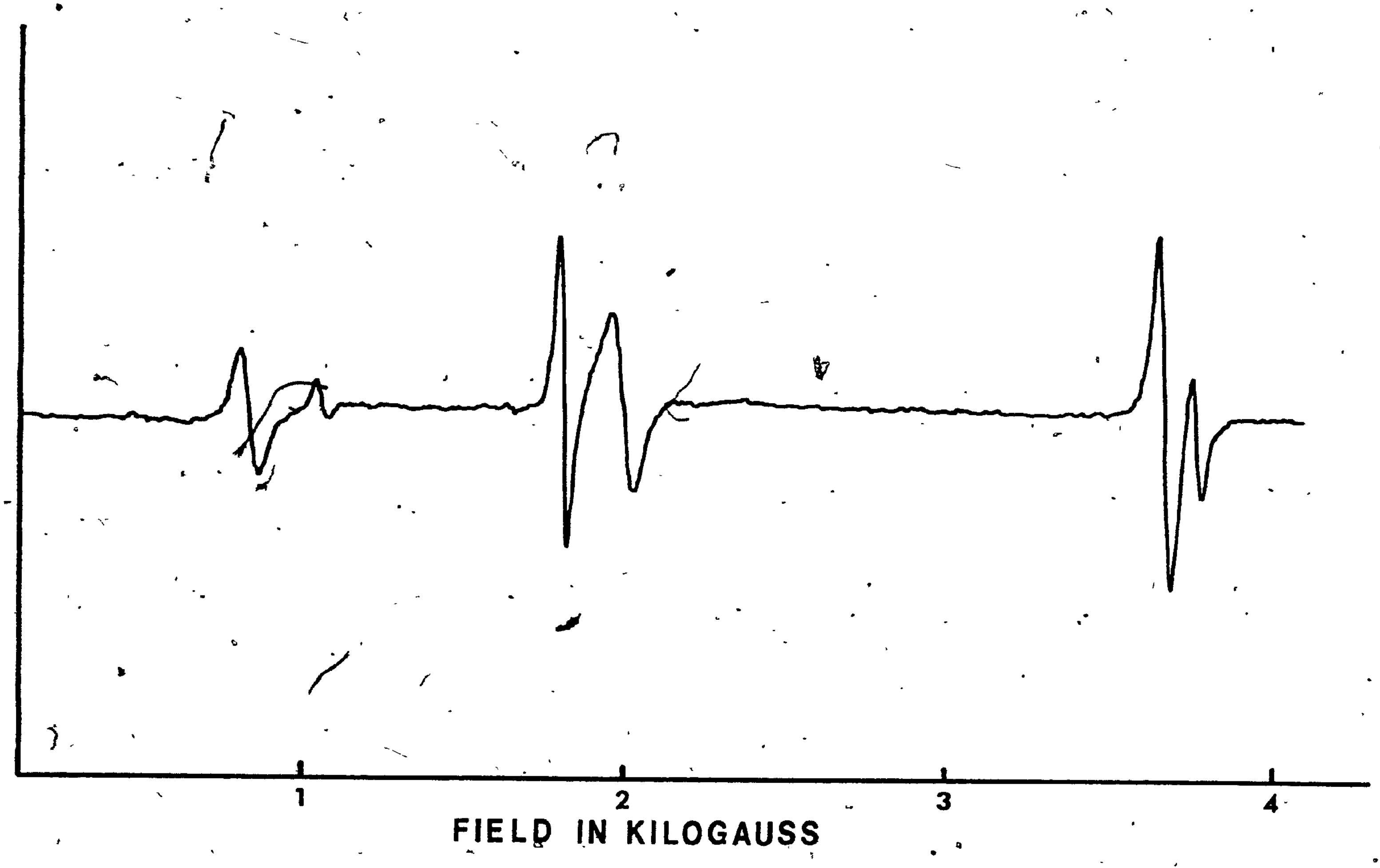

Fig. 6.6. EPR absorption spectrum with the static magnetic field directed along the c-axis.

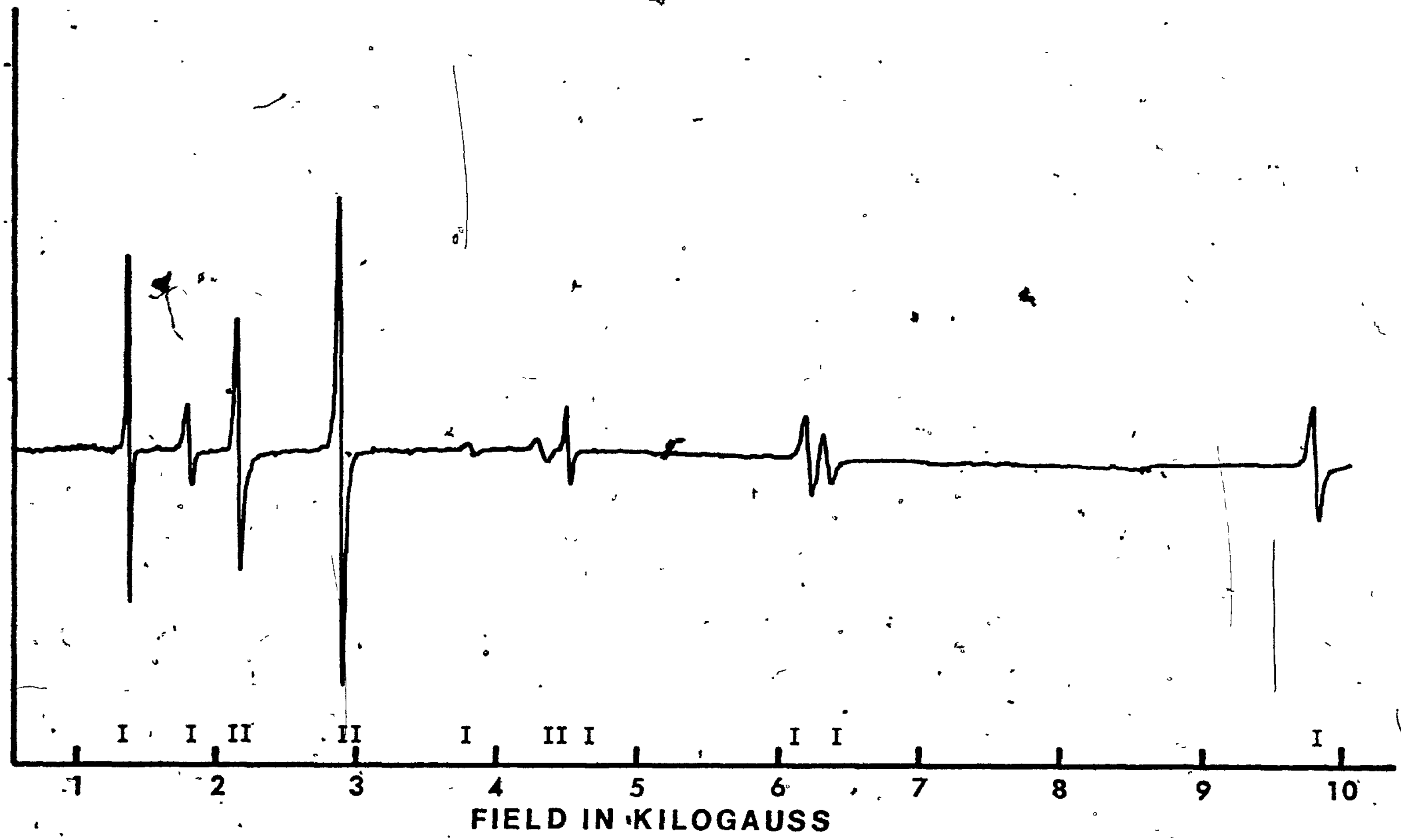

Fig. 6.7. EPR absorption spectrum with the static magnetic field directed along the Z_I-axis. Lines are identified for each site by I and II .

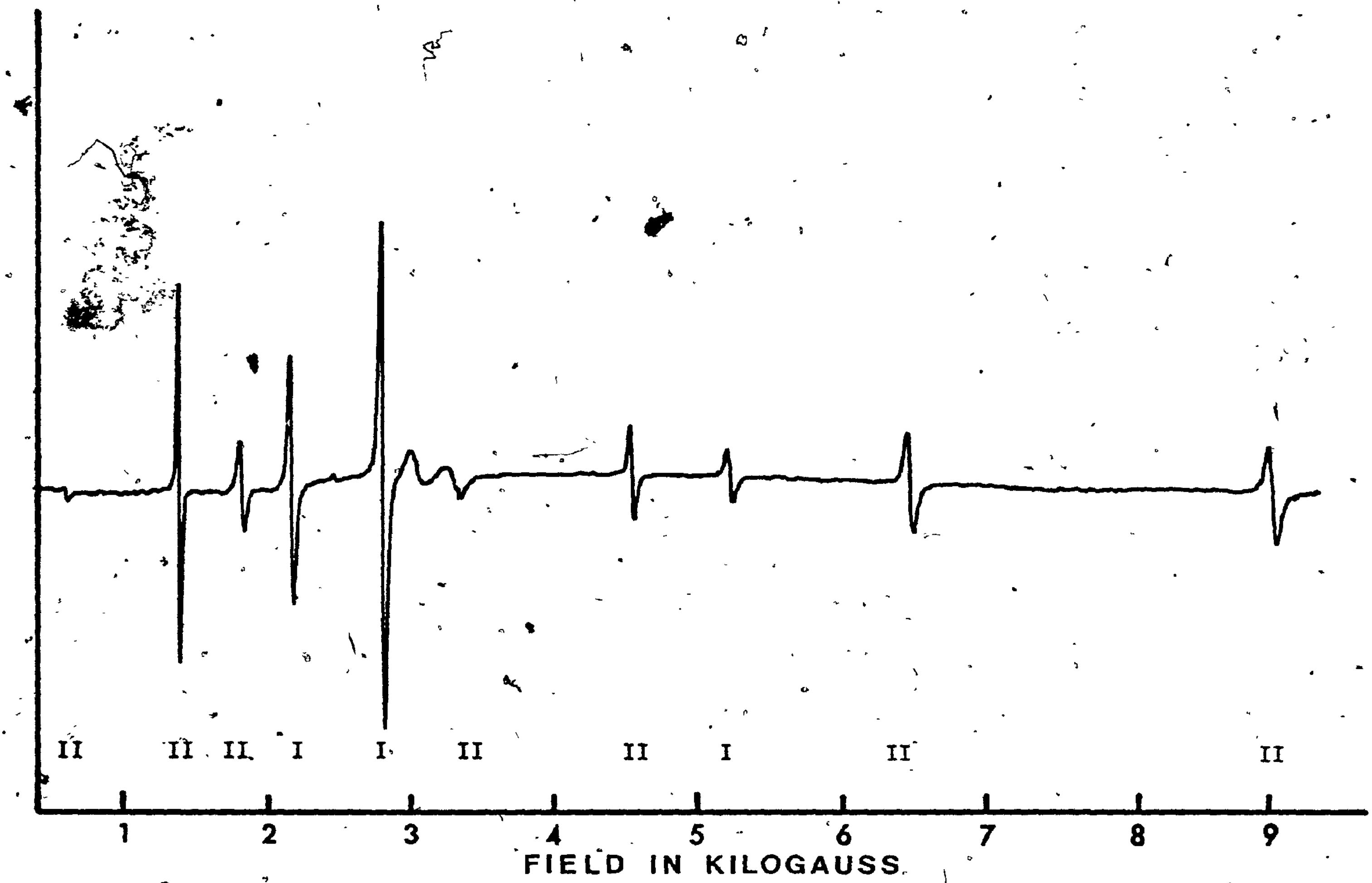

Fig. 6.8. EPR absorption spectrum with the static magnetic field directed along the Y_I-axis. Lines are identified for each site by I and II.

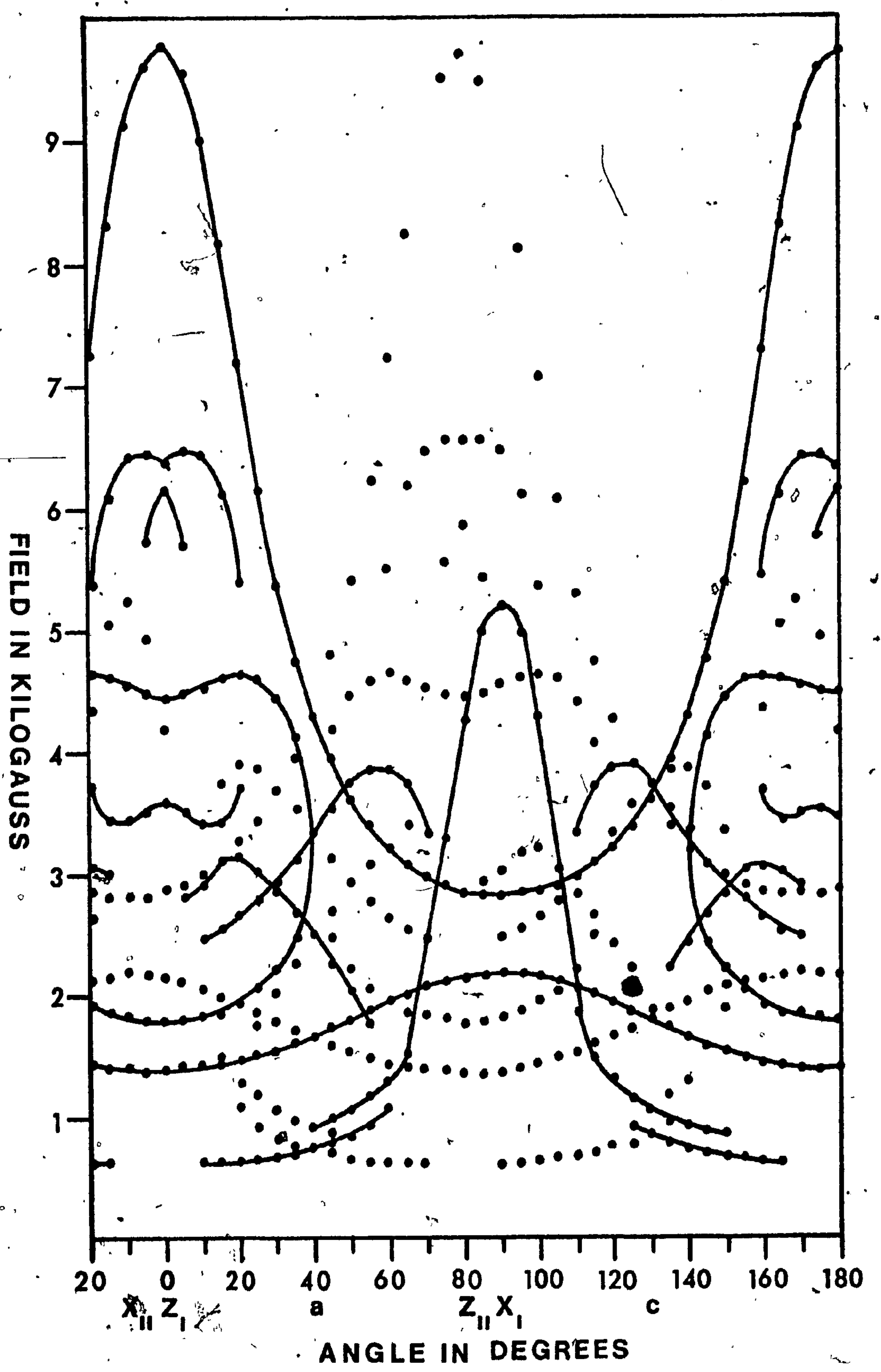

Fig. 6.9. The spectral angular variation for the static magnetic field in the ac plane.

fitted. Thus a total of forty-nine and forty-six lines are used for site I and site II respectively. The values of the parameters g_{xx}, g_{yy}, g_{zz}, b_2^0, b_2^2, b_4^0, b_4^2 and b_4^4 which characterize the EPR data are listed in Table 6.1. The initial values for the least-squares fitting procedure were those given by Amitay for g_{xx}, g_{yy}, g_{zz}, b_2^0 and b_2^2, the remaining parameters were put equal to zero.

Table 6.1. Values of the parameters characterizing the EPR data for Fe^{3+} in $(NH_4)_2InCl_5 \cdot H_2O$ at 9.4434 gHz at 295 K. The units of the non-Zeeman parameters are gHz. Here $b_2^m = 3B_2^m$ and $b_4^m = 60B_4^m$. The values enclosed in brackets are those determined by Amitay.

	SITE I	SITE II	
g_{zz}	2.014 ±.003	2.015 ±.003	(2.003)
g_{xx}	2.016 ±.003	2.015 ±.003	(2.003)
g_{yy}	2.014 ±.003	2.008 ±.003	(2.003)
b_2^0	-4.570 ±.008	-4.563 ±.008	(-4.561)
b_2^2	2.545 ±.008	2.547 ±.008	(2.565)
b_4^0	0.027 ±.008	0.028 ±.008	(0.0006)
b_4^2	0.032 ±.008	0.033 ±.008	(0.0003)
b_4^4	0.137 ±.008	0.150 ±.008	(0.0058)
SSMD	0.1259	0.0957	-

Inspection of the parameters for each site show that all the parameters are the same within experimental errors, as expected.

Using the parameters for site I given in Table 6.1 the variations of eigenvalues as functions of static magnetic field along the a-axis, b-axis (X-axis), c-axis, Z-axis and Y-axis are shown in Figs. 6.10 to 6.14 respectively. The zero field splitting at room temperature are as follows (the same for the two sites). E(±1/2) = 13.69 ± .10 gHz, E(±3/2) = 1.78 ± .10 gHz, E(±5/2) = -15.47 ± .10 gHz (the numbers in parentheses represent magnetic quantum numbers).

Tables 6.2 and 6.3 list the magnetic field values of the lines measured at each orientation of the static magnetic field and the SMD for site I and site II respectively.

Table 6.2. The magnetic field of each line at various orientations of the static magnetic field and the SMD. The angles represent the orientation in the ZY plane as measured from the Z-axis for site I and X represents the lines measured along the X-axis.

Angle (Degrees)	Magnetic Field (Gauss)	SMD (gHz^2)
X	8507	$.455 \times 10^{-3}$
X	3923	$.605 \times 10^{-3}$
X	1934	$.461 \times 10^{-3}$
X	1609	$.232 \times 10^{-3}$
X	758	$.186 \times 10^{-1}$

Table 6.2 Cont'd

Angle (Degrees)	Magnetic Field (Gauss)	SMD (gHz^2)
X	650	$.521 \times 10^{-3}$
X	293	$.157 \times 10^{-3}$
0	9802	$.162 \times 10^{-5}$
0	6349	$.372 \times 10^{-1}$
0	6194	$.235 \times 10^{-1}$
0	4492	$.244 \times 10^{-3}$
0	1804	$.130 \times 10^{-3}$
0	1377	$.838 \times 10^{-4}$
20	7223	$.252 \times 10^{-2}$
20	5429	$.134 \times 10^{-2}$
20	4676	$.138 \times 10^{-3}$
20	2660	$.548 \times 10^{-3}$
20	1934	$.101 \times 10^{-1}$
20	1447	$.144 \times 10^{-4}$
20	620	$.421 \times 10^{-4}$
30	5412	$.472 \times 10^{-4}$
30	4486	$.729 \times 10^{-3}$
30	2956	$.224 \times 10^{-2}$
30	2226	$.157 \times 10^{-3}$
30	1535	$.929 \times 10^{-7}$
30	635	$.308 \times 10^{-2}$
40	4354	$.338 \times 10^{-3}$

Table 6.2 Cont'd

Angle (Degrees)	Magnetic Field (Gauss)	SMD (gHz^2)
40	3350	$.553 \times 10^{-3}$
40	2499	$.267 \times 10^{-2}$
40	1651	$.330 \times 10^{-3}$
40	904	$.670 \times 10^{-2}$
40	691	$.331 \times 10^{-2}$
50	3758	$.338 \times 10^{-4}$
50	3665	$.133 \times 10^{-5}$
50	2031	$.130 \times 10^{-2}$
50	1797	$.128 \times 10^{-4}$
50	1053	$.167 \times 10^{-2}$
50	813	$.249 \times 10^{-3}$
60	3907	$.639 \times 10^{-4}$
60	3258	$.803 \times 10^{-5}$
60	1941	$.573 \times 10^{-4}$
60	1297	$.273 \times 10^{-3}$
60	1060	$.617 \times 10^{-3}$
70	3386	$.575 \times 10^{-4}$
70	3010	$.111 \times 10^{-4}$
70	2068	$.237 \times 10^{-3}$
90	5270	$.464 \times 10^{-4}$
90	2836	$.105 \times 10^{-4}$
90	2190	$.110 \times 10^{-2}$

Table 6.3. The magnetic field of each line at various orientations of the static magnetic field and the SMD. The angles represent the orientation in the ZY plane as measured from the Z-axis for site II and X represents the lines along the X-axis.

Angle (Degrees)	Magnetic Field (Gauss)	SMD (gHz^2)
X	8507	$.378 \times 10^{-3}$
X	3923	$.982 \times 10^{-3}$
X	1934	$.288 \times 10^{-3}$
X	1609	$.486 \times 10^{-3}$
X	758	$.183 \times 10^{-1}$
X	650	$.367 \times 10^{-3}$
X	293	$.971 \times 10^{-4}$
0	9733	$.203 \times 10^{-1}$
0	4489	$.162 \times 10^{-2}$
0	1806	$.172 \times 10^{-2}$
0	1379	$.472 \times 10^{-3}$
20	7249	$.166 \times 10^{-2}$
20	5546	$.804 \times 10^{-2}$
20	4682	$.152 \times 10^{-2}$
20	2651	$.208 \times 10^{-3}$
20	1941	$.113 \times 10^{-2}$
20	1443	$.233 \times 10^{-4}$
20	606	$.152 \times 10^{-2}$
30	5453	$.574 \times 10^{-3}$

Table 6.3 Cont'd

Angle (Degrees)	Magnetic Field (Gauss)	SMD (gHz^2)
30	4508	$.128 \times 10^{-2}$
30	2923	$.649 \times 10^{-2}$
30	2210	$.277 \times 10^{-4}$
30	1532	$.169 \times 10^{-3}$
30	639	$.174 \times 10^{-2}$
40	4354	$.165 \times 10^{-3}$
40	3350	$.177 \times 10^{-4}$
40	2499	$.104 \times 10^{-2}$
40	1651	$.356 \times 10^{-3}$
40	904	$.200 \times 10^{-2}$
40	691	$.308 \times 10^{-2}$
50	3696	$.121 \times 10^{-2}$
50	2046	$.122 \times 10^{-2}$
50	1789	$.914 \times 10^{-3}$
50	1054	$.136 \times 10^{-5}$
50	800	$.119 \times 10^{-2}$
60	3900	$.203 \times 10^{-2}$
60	3279	$.410 \times 10^{-3}$
60	1934	$.718 \times 10^{-3}$
60	1288	$.746 \times 10^{-3}$
60	1058	$.386 \times 10^{-3}$
70	3439	$.283 \times 10^{-2}$

Table 6.3 Cont'd

Angle (Degrees)	Magnetic Field (Gauss)	SMD (gHz^2)
70	3026	$.146 \times 10^{-4}$
70	2062	$.460 \times 10^{-3}$
90	5261	$.687 \times 10^{-2}$
90	2844	$.375 \times 10^{-3}$
90	2186	$.176 \times 10^{-4}$

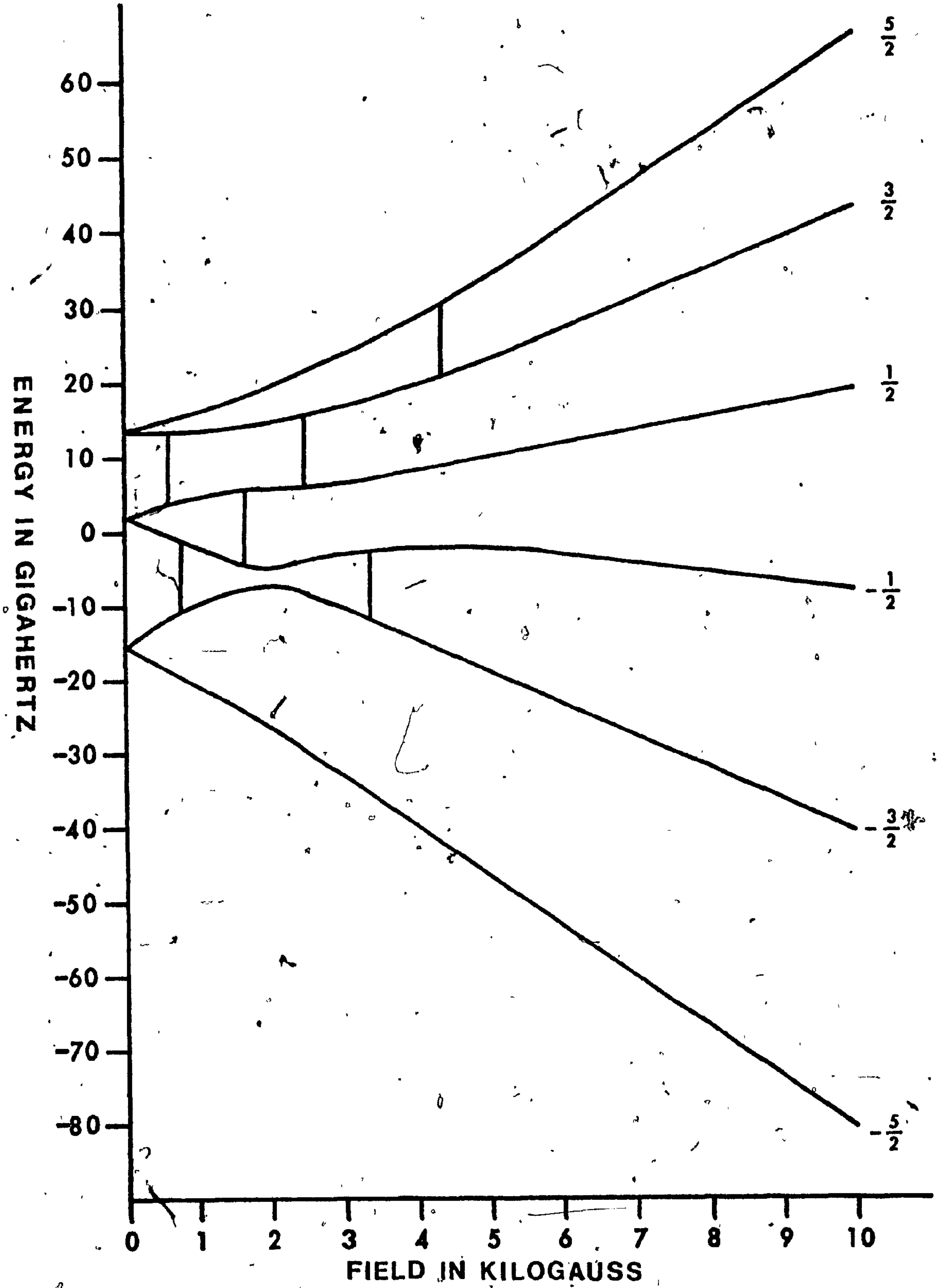

Fig. 6.10. The variations of eigenvalues as functions of static magnetic field directed along the a-axis.

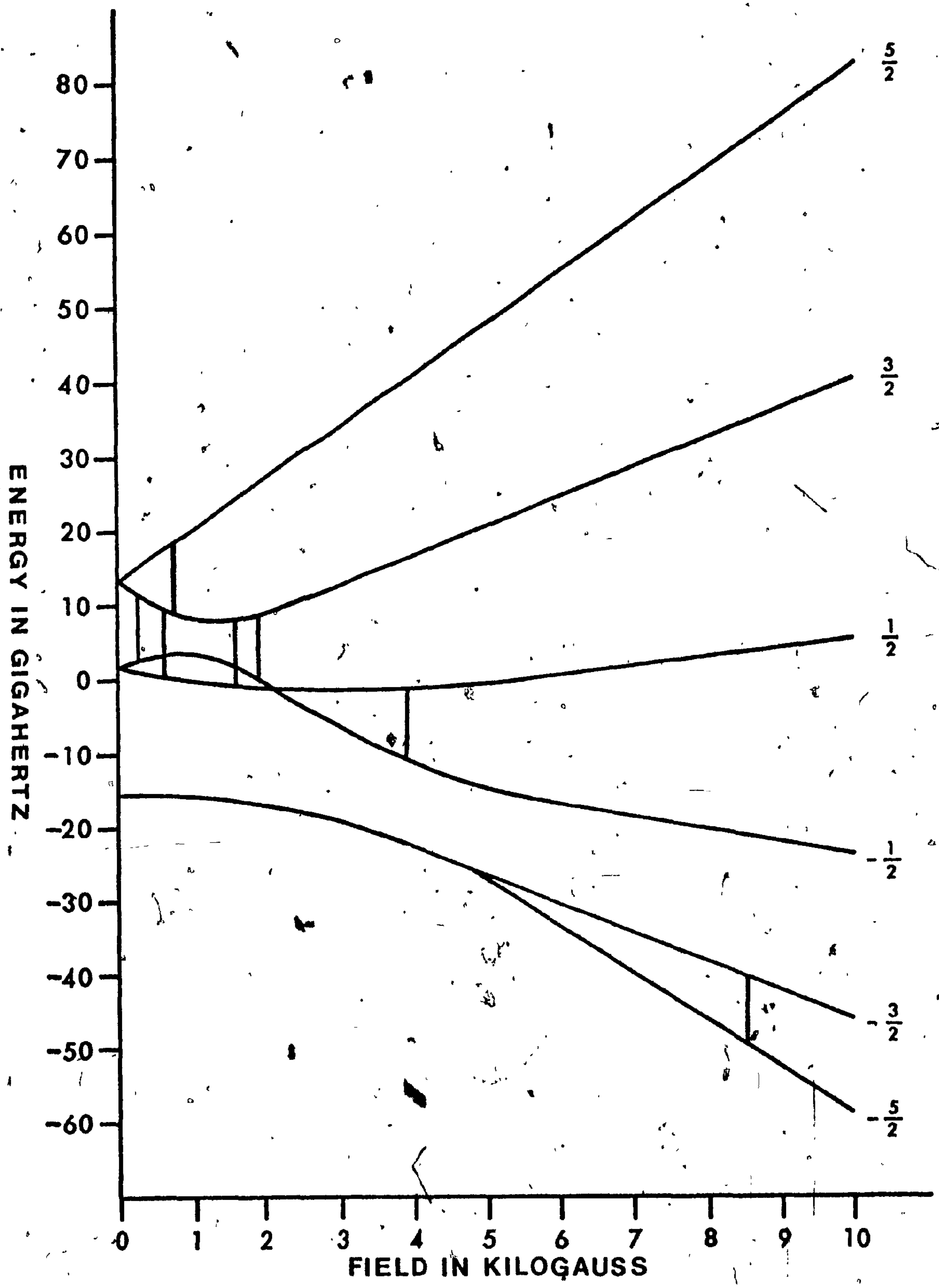

Fig. 6.11. The variations of eigenvalues as functions of static magnetic field directed along the b-axis (X-axis).

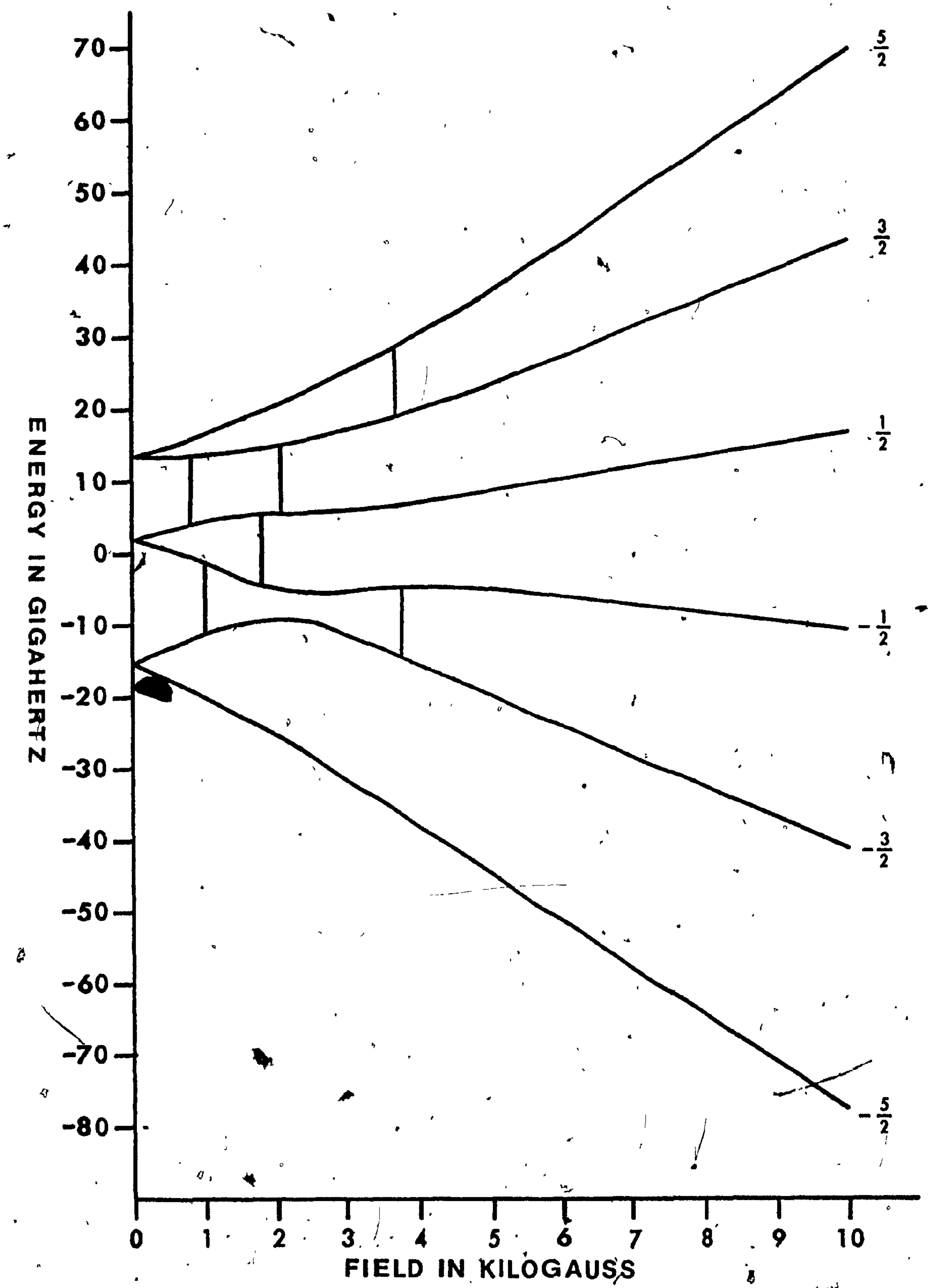

Fig. 6.12. The variations of eigenvalues as functions of static magnetic field directed along the c-axis.

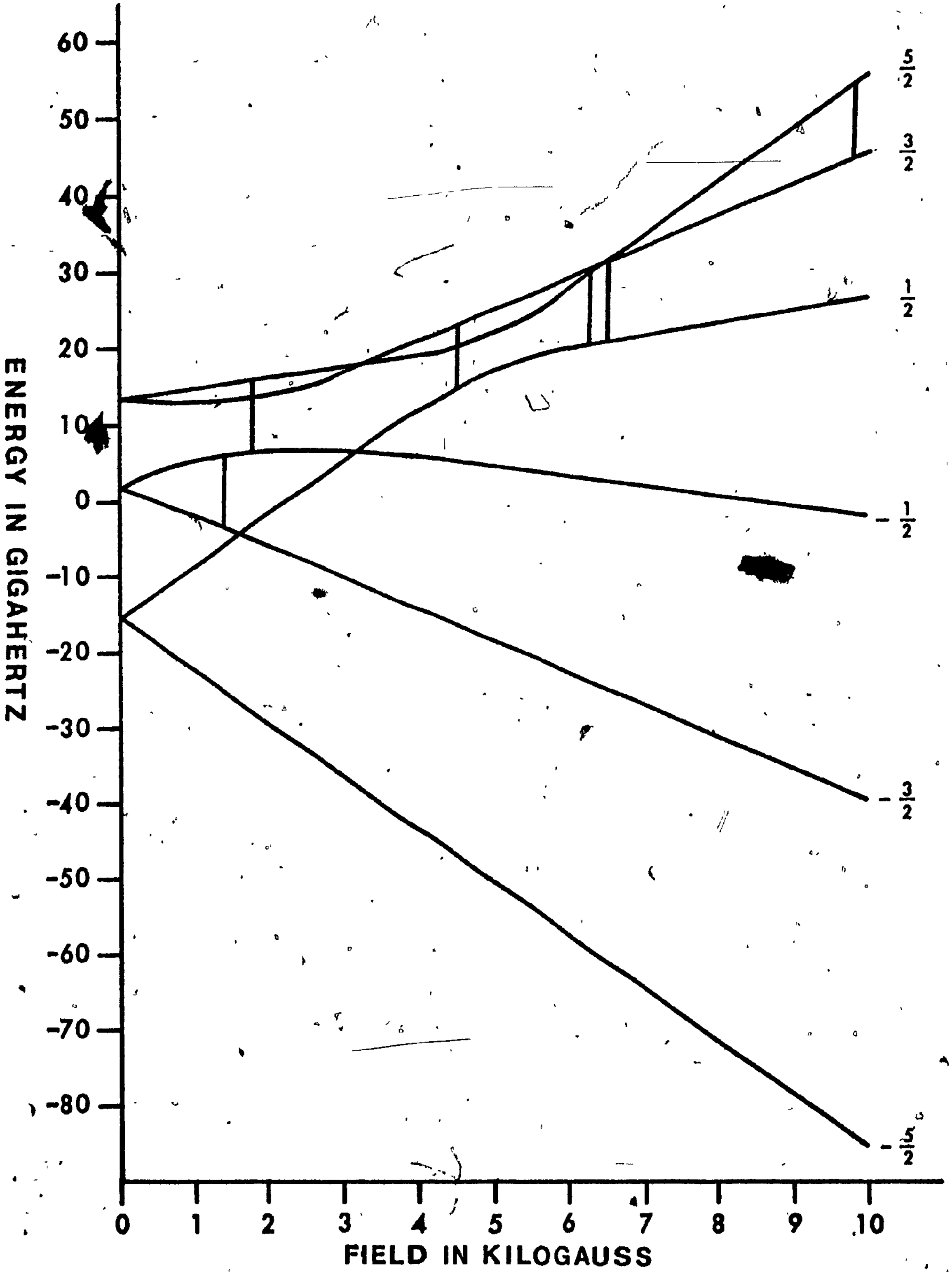

Fig. 6.13. The variations of eigenvalues as functions of static magnetic field directed alongthe Z-axis.

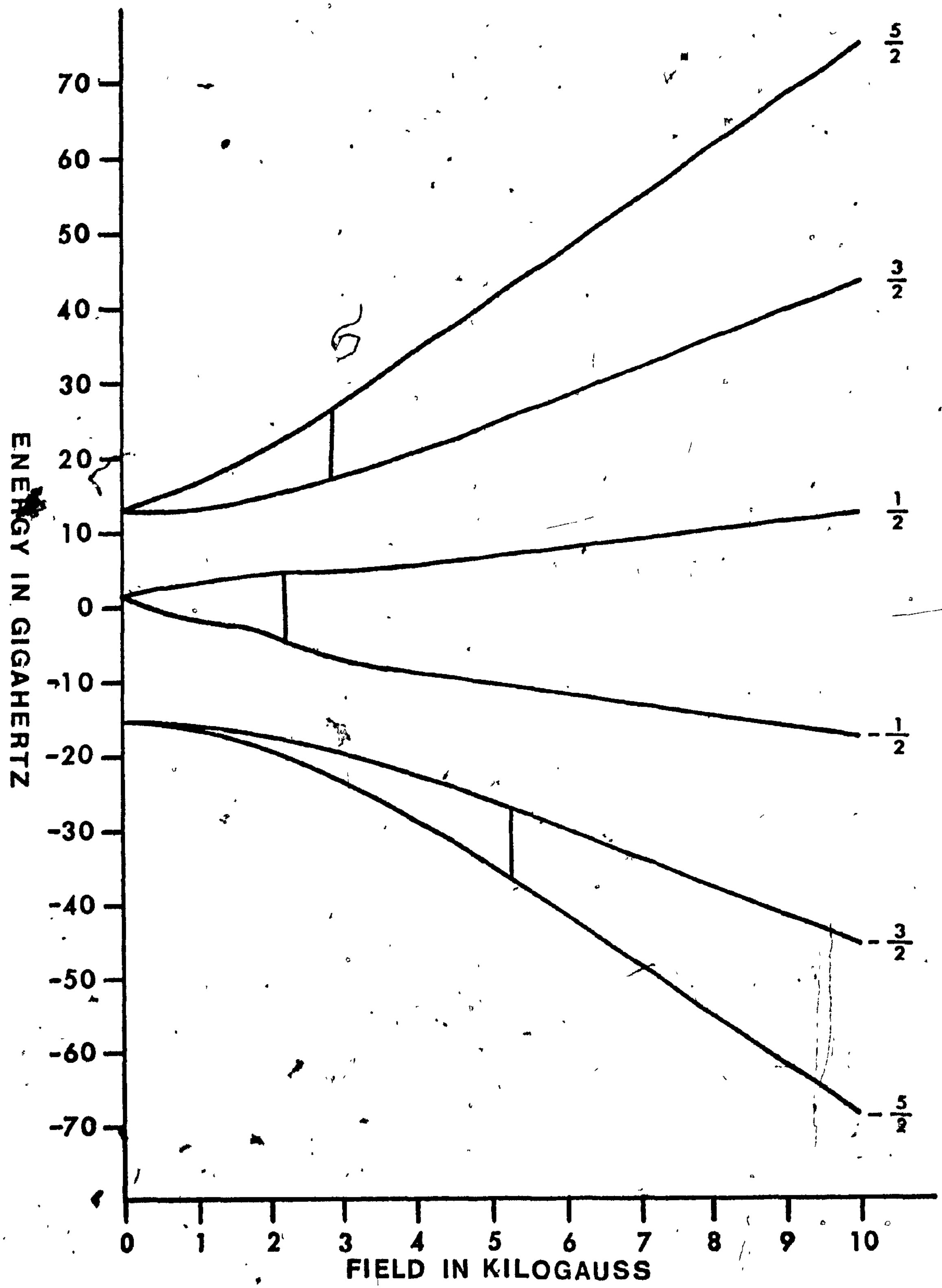

Fig. 5.14. The variations of eigenvalues as functions of static magnetic field directed along the Y-axis.

CHAPTER VII

CONCLUSIONS

An EPR study of Fe^{3+} in guanidinium aluminum sulfate hexahydrate and in di-ammonium indium pentachloride monohydrate has been presented. From an experimental point of view the Fe^{3+} in GASH sample using enriched Fe^{57} rather than natural iron appears more suitable for the detection of dynamically oriented nuclei for obvious reasons. The crystals grow in thin plates and can be grown to diameters of one inch with relative ease, making very suitable Mossbäuer absorbers. In addition, the crystals of GASH have easily identifiable faces.

The values of all the spin Hamiltonian parameters are calculated using a rigorous least-squares fitting procedure. The parameters for Fe^{3+} in GASH at various temperatures are presented in Tables 5.3, 5.7 and 5.11. The Tables show significantly different parameters from those obtained by other researchers, as well the low temperature data provides the necessary information to determine the sign of the zero field splitting parameter B_2^0, which turns out to be negative.

Table 6.1 gives the parameters for Fe^{3+} in $(NH_4)_2InCl_5 \cdot H_2O$. The most significant difference in the parameters quoted here being the values of B_4^m (m = 0,2,4), which are here determined rather accurately because of the large number of magnetic resonance transitions used in the least-squares fitting procedure to calculate the parameters. The data also clearly exhibits the existence of two magnetically inequivalent sites of Fe^{3+} in the unit cell and that their Z-axes which lie in the ac-plane make angles of ±(40.00 ± 0.25°) with the a-axis.

APPENDIX I

Values of parameters and the corresponding SMD values in the various iterations of the brute-force method for Gd^{3+} in $SmCl_3 \cdot 6H_2O$.

Parameters	g_{xx}	g_{yy}	b_2^0	b_2^2	b_4^0	b_4^2
Initial Values	1.98580	1.97649	1.85589	-1.05178	-0.02094	0.00000
Increment/step	0.01	0.01	0.05	0.05	0.05	0.05
n factor	6	6	6	6	3	3
f factor	4	4	4	4	2	2
Iteration 1	1.98580	1.97649	1.85589	-1.10178	-0.02905	0.05000
Iteration 2	1.98830	1.98899	1.86839	-1.10178	-0.02905	0.05000
Iteration 3	1.99143	1.99024	1.86839	-1.10490	-0.02905	0.03750
Iteration 4	1.99143	1.99024	1.86995	-1.10647	-0.03530	0.02500
Iteration 5	1.99123	1.99044	1.87093	-1.10744	-0.03217	0.02500
Iteration 6	1.99128	1.99049	1.87117	-1.10769	-0.03217	0.02656
Iteration 7	1.99129	1.99050	1.87123	-1.10775	-0.03295	0.02656
Increment/step	0.001	0.001	0.005	0.005	0.005	0.005
Iteration 8.	1.99129	1.99150	1.87123	-1.11275	-0.03295	0.02656
Iteration 9	1.99129	1.99200	1.87123	-1.11400	-0.03295	0.02656
Iteration 10	1.99142	1.99231	1.87061	-1.11462	-0.03295	0.02781
Iteration 11	1.99134	1.99231	1.87086	-1.11431	-0.03295	0.02844
Iteration 12	1.99132	1.99231	1.87077	-1.11421	-0.03295	0.02844
Iteration 13	1.99132	1.99230	1.87230	-1.11410	-0.03311	0.02844
Iteration 14	1.99132	1.99230	1.87065	-1.11419	-0.03311	0.02837

Appendix I Cont'd

b_4^4	b_6^0	b_6^2	b_6^4	b_6^6	SMD
0.00000	-0.00204	0.00000	0.00000	0.00000	0.27030
0.05	0.05	0.05	0.05	0.05	
3	3	3	3	3	
2	2	2	2	2	
0.00000	-0.00204	0.05000	0.05000	0.05000	0.06530
0.00000	-0.00204	0.02500	0.02500	0.02500	0.02635
0.00000	-0.00204	0.00000	0.00000	0.00000	0.01746
0.00625	-0.00204	0.00000	0.00000	0.00000	0.01490
0.00000	0.00108	0.00625	0.00000	-0.00625	0.00231
0.00156	0.00108	0.00938	0.00313	-0.00469	0.00206
0.00234	0.00108	0.01094	0.00469	-0.00313	0.00180
0.005	0.01	0.01	0.01	0.01	
0.00234	0.00108	0.02094	0.01469	0.00688	0.00600
0.00016	0.00108	0.02594	0.02469	0.01188	0.00041
0.00109	0.00108	0.02894	0.02719	0.01438	0.00035
0.00109	0.00108	0.02844	0.02844	0.01563	0.00033
0.00078	0.00108	0.02844	0.02844	0.01500	0.00033
0.00109	0.00108	0.02844	0.02875	0.01563	0.00031
0.00109	0.00108	0.02875	0.02906	0.01594	0.00031

BIBLIOGRAPHY

1. S. K. Misra and W. A. Barker, Phys. Rev., 138 , A58 (1965) .
2. S. K. Misra and J. M. Daniels, Can. J. Phys., 43, 1843 (1965) .
3. E. G. Brock, D. Stripe and E. I. Hormats, J. Chem. Phys., 37, 2735 (1962) .
4. R. W. Schwartz and R. L. Carlin, J. Am. Chem. Soc., 92 6763 (1970) .
5. S. K. Misra, J. Mag. Res., In Press.
6. H. L. Wesemeyer 1962 Ph.D. thesis (University of British Columbia, Vancouver, Canada) .
7. M. Amitay 1966 Ph.D. thesis (Carnegie Institute of Technology, Pittsburgh, U.S.A.).
8. A. Abragam and B. Bleaney, Electron Paramagnetic Resonance of Transition Ions, Clarendon Press, Oxford (1970) .
9. C. P. Poole and H. A. Farach, The Theory of Magnetic Resonance, John Wiley and Sons, New York (1972) .
10. S. Geller and D. P. Booth, Z. Krist., 117, 3 (1958) .
11. Z. I. Ezhkova, G. S. Zhdanov and M. M. Umanskii, Kristallografiya, 3, 231 (1958) . (Translation, Soviet Phys. - Cryst. 3, 230 (1958)) .
12. D. W. McCall, J. Chem. Phys., 26, 706 (1957) .
13. B. Bleaney and R. S. Trenam, Proc. Roy. Soc. (London) , A223, 1 (1954) .
14. H. P. Klug, E. Kummer and L. Alexander, J. Am. Chem. Soc. 70, 3064 (1948) .

15. V. M. Vinokurov et al., Soviet Phys. - Solid State, English translation 3, 1797 (1962).

16. M. Weger and W. Low, Phys. Rev., 111, 1526 (1958).

17. G. Feher, Bell System Tech. J., 36, 449 (1957).

18. C. P. Poole, Electron Spin Resonance, John Wiley and Sons, New York (1967).

19. G. R. Sharp and S. K. Misra, Rev. Sci. Instrum., 44 1777 (1973).

20. G. R. Sharp 1972 M.Sc. thesis (Sir George Williams University, Montreal, Canada).

21. H. A. Buckmaster, R. Chatterjee, J. C. Dering, D. J. I. Fry, Y. H. Shing, J. D. Skirrow and B. Venkatesan, J. Mag. Res., 4, 113 (1971).

22. S. K. Misra and G. R. Sharp, J. Mag. Res., In Press.

23. S. K. Misra and G. R. Sharp, J. Phys C, 9, 401 (1976).

24. S. K. Misra and G. R. Sharp, J. Chem. Phys., 64, 2168 (1976).

25. S. K. Misra and G. R. Sharp, J. Phys. Chem. Solids, In Press.

26. S. K. Misra and G. R. Sharp, Phys. Stat. Solidii, 75, 607, (1976).

27. S. K. Misra and G. R. Sharp, J. Phys. C, 9, 1975 (1976).

28. S. K. Misra and G. R. Sharp, Physica, B, 83, 174 (1976).